Frontiers of Information Technology & Electronic Engineering
www.jzus.zju.edu.cn; engineering.cae.cn; www.springerlink.com
ISSN 2095-9184 (print); ISSN 2095-9230 (online)
E-mail: jzus@zju.edu.cn

Review:

Synaptic devices based on semiconductor nanocrystals*

Mingxuan BU[1,2], Yue WANG[1,2], Lei YIN[1,2], Zhouyu TONG[1,2], Yiqiang ZHANG[3], Deren YANG[1,2,4,5], Xiaodong PI[†‡1,2,4,5]

[1]*State Key Laboratory of Silicon Materials, Zhejiang University, Hangzhou 310027, China*
[2]*School of Materials Science and Engineering, Zhejiang University, Hangzhou 310027, China*
[3]*School of Material Science and Engineering, Zhengzhou University, Zhengzhou 450001, China*
[4]*Institute of Advanced Semiconductors, Hangzhou Innovation Center, Zhejiang University, Hangzhou 311200, China*
[5]*Zhejiang Provincial Key Laboratory of Power Semiconductor Materials and Devices, Hangzhou Innovation Center, Zhejiang University, Hangzhou 311200, China*
[†]E-mail: xdpi@zju.edu.cn

Received Nov. 29, 2021; Revision accepted Apr. 24, 2022; Crosschecked June 8, 2022; Published online Sept. 6, 2022

Abstract: To meet a growing demand for information processing, brain-inspired neuromorphic devices have been intensively studied in recent years. As an important type of neuromorphic device, synaptic devices have attracted strong attention. Among all the kinds of materials explored for the fabrication of synaptic devices, semiconductor nanocrystals (NCs) have become one of the preferred choices due to their excellent electronic and optical properties. In this review, we first introduce the research background of synaptic devices based on semiconductor NCs and briefly present the basic properties of semiconductor NCs. Recent developments in the field of synaptic devices based on semiconductor NCs are then discussed according to the materials employed in the active layers of the devices. Finally, we discuss existing problems and challenges of synaptic devices based on semiconductor NCs.

Key words: Semiconductor nanocrystal; Synaptic devices; Neuromorphic computing
https://doi.org/10.1631/FITEE.2100551 **CLC number:** Q811; TN303

1 Introduction

In recent years, the rate of the development of information technology has been increasingly rapid. New areas such as artificial intelligence increasingly demand novel hardware systems for computing (Turing, 1950; Searle, 1980; Block, 1981). Although current computers based on the so-called von Neumann architecture possess unparalleled strength in solving complex mathematical problems (Merolla et al., 2014; Upadhyay et al., 2016; Zidan et al., 2018), their operation efficiency is limited by the transfer of data between a separated memory and processor (Gkoupidenis et al., 2017; Liu CS et al., 2018; Manipatruni et al., 2018). Further, computers based on the von Neumann architecture do not distinguish between instruction data, leading to the overall processing speed being seriously restricted by the speed of access to memory (Wang Y et al., 2021). It has also become clear that computers are increasingly hungry for energy because ever-decreasing device sizes increase the quantity of devices in a fixed area, causing energy consumption to soar (Indiveri et al., 2006). It is well-recognized that a biological neural system has the characteristics of high parallelism, high fault tolerance,

‡ Corresponding author
* Project supported by the National Key Research and Development Program of China (No. 2018YFB2200101) and the National Natural Science Foundation of China (Nos. 91964107, U20A20209, and 61721005)
ORCID: Mingxuan BU, https://orcid.org/0000-0001-7929-4870; Xiaodong PI, https://orcid.org/0000-0002-4233-6181

and low energy consumption (Attwell and Laughlin, 2001; Machens, 2012; Prezioso et al., 2015; Esser et al., 2016). Hence, an architecture that simulates a biological neural system (Yin et al., 2020) is considered to be well-suited to address the issues faced by the current computers based on the von Neumann architecture.

Computing enabled by an architecture simulating a biological neural system (i.e., an artificial neural network) is called neuromorphic computing. Because information is transferred via synapses in a biological neural system (Ni et al., 2019), synaptic devices that mimic the functionalities of synapses play a critical role in an artificial neural network (van de Burgt et al., 2018; Zidan et al., 2018; Tang et al., 2019). To date, various materials have been investigated for the fabrication of synaptic devices (Lin et al., 2020; Hu H et al., 2021; Li YY et al., 2021; Zeng et al., 2021), and semiconductor nanocrystals (NCs) have become one of the preferred material choices due to their excellent electronic and optical properties (Guo et al., 1997; Erogbogbo et al., 2011; Holman and Kortshagen, 2011; Zhou et al., 2016). Synaptic devices based on semiconductor NCs exhibit varying performance, which may be tuned by the size, surface, and components of semiconductor NCs (Heitmann et al., 2005; Norris et al., 2008; Ma YS et al., 2012; Wang R et al., 2012; Dasog et al., 2014; Boles et al., 2016; Arduca and Perego, 2017; Marri et al., 2017). Si NCs (Dohnalová et al., 2014; Liu XK et al., 2016; Ni et al., 2017), transition metal chalcogenide NCs (Semonin et al., 2010; Zhang H et al., 2017), and perovskite NCs (Wang Y et al., 2018; Periyal et al., 2020) have been the typical semiconductor NCs used in synaptic devices. Impressive features such as light programming with electric erasing (Wang Y et al., 2018), ultrasensitive light-response (Pradhan et al., 2020), and temperature-facilitated modulation of synaptic plasticity (Li EL et al., 2019) have been realized with synaptic devices based on semiconductor NCs.

In this review, we introduce the basic properties of semiconductor NCs and present recent developments of synaptic devices based on semiconductor NCs in the form of films and heterostructures. Challenges and future trends in the development of synaptic devices based on semiconductor NCs are discussed.

2 Basic properties of semiconductor nanocrystals (NCs)

The special properties of NCs are largely derived from their rich surface states induced by their small size (Heitmann et al., 2005; Boles et al., 2016). The electronic structure of semiconductor NCs is significantly different from that of corresponding bulk materials because of the quantum confinement effect (Kagan et al., 2016). In contrast to the continuous band in bulk semiconductor materials, the electronic structure of ideal NCs is close to discrete levels. Because the energy band is produced by the energy-level splitting of tightly bonded atoms, the size of a NC determines the degree of energy-level splitting and then the energy gap between adjacent states (the highest occupied and lowest unoccupied states) (Ekimov et al., 1985).

The properties of semiconductor NCs can be significantly affected by the size effect, doping effect, and surface state. Owing to the quantum confinement effect, the band gap of NCs increases with a decrease in their size, leading to a blue shift of emission and absorption (Heitmann et al., 2005; Mastronardi et al., 2012). Occupying the surface states with different ligands can effectively modify the electronic structure and further, the chemical stability and luminescence of NCs (Ma YS et al., 2012; Wang R et al., 2012; Dasog et al., 2014). Doping as a common means of functional modification can affect the performance of NCs by changing both the size and the surface (Norris et al., 2008; Arduca and Perego, 2017; Marri et al., 2017).

With these modulation methods, the tuning of light absorption/emission is achievable, providing broad application prospects for semiconductor NCs in optical-related industries. Some other optical properties also contribute to the application of NCs. For example, the carrier multiplication effect (i.e., the absorption of a single photon by a NC can generate multiple excitons with an efficiency of up to 100% under the condition that pump photon energies are high enough) (Schaller and Klimov, 2004; Schaller et al., 2005) renders NCs a promising material for application in many fields, such as solar cells, photoelectric memory, and low-threshold lasers.

2.1 Size effect

One of the most important properties of semiconductors is the band gap, which largely determines their electronic and optical properties. As the size of semiconductor NCs decreases, the split extent of the electron step declines, causing the band gap to be closer to the difference between the highest occupied molecular orbital (HOMO) and the lowest unoccupied molecular orbital (LUMO). Fig. 1a shows experimental evidence of the influence being exerted by a NC's size on its band gap.

The relationship between the band gap and the size of NCs can now be described quantitively. Singh et al. (2018) formulated a model of size-dependent band-gap energy of semiconductor NCs:

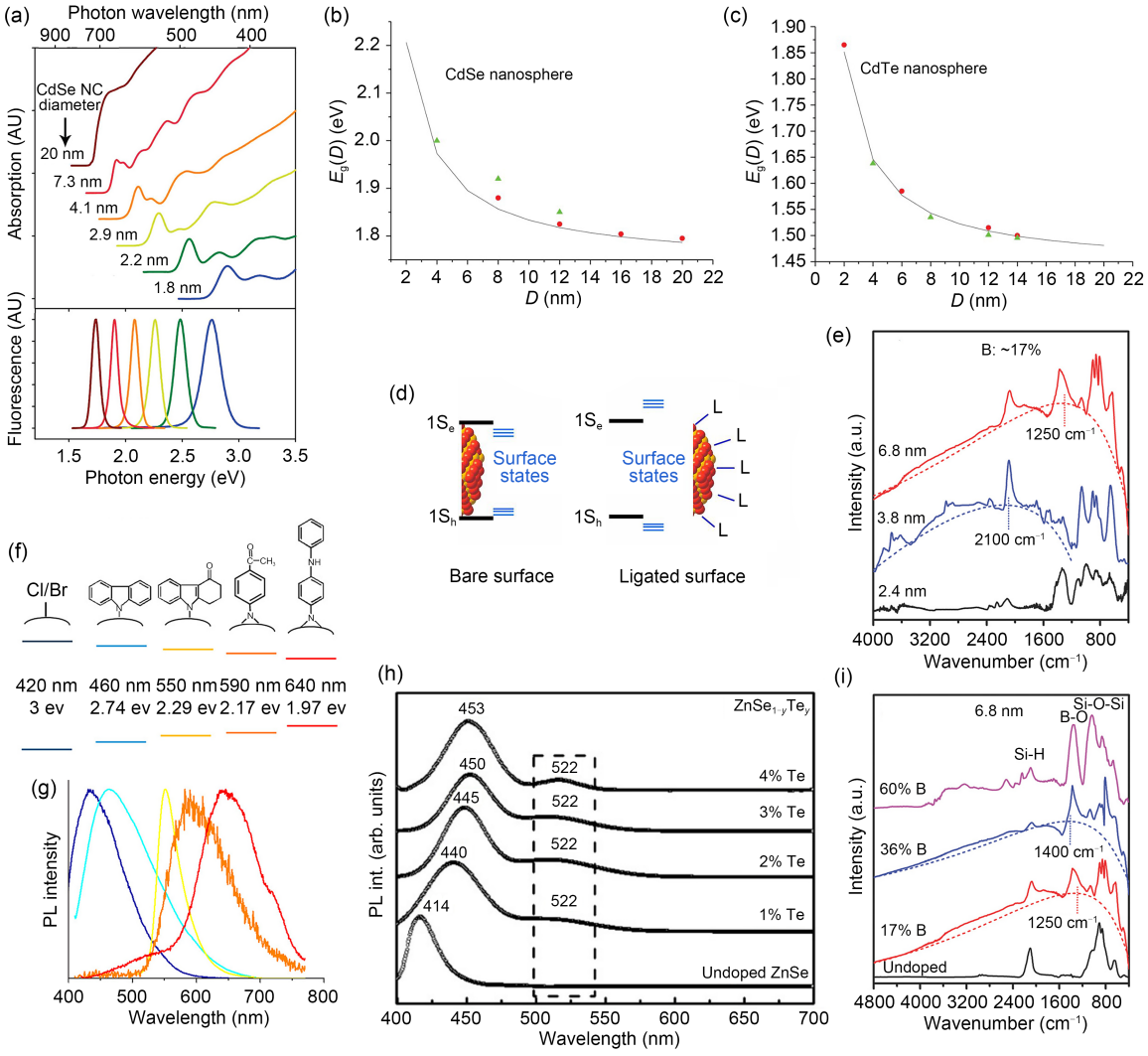

Fig. 1 (a) Absorption and fluorescence spectra of CdSe NCs (Reprinted from Smith and Nie (2010), Copyright 2010, with permission from American Chemical Society); variation of energy band gap of CdSe (b) and CdTe (c) NCs with size (Reprinted from Singh et al. (2018), Copyright 2018, with permission from the authors, licensed under CC BY 4.0); (d) change in energy of surface states before and after being occupied (Reprinted from Kagan et al. (2016), Copyright 2016, with permission from the American Association for the Advancement of Science); (e) Fourier transform infrared (FTIR) spectra of hyperdoped silicon NCs with different sizes of 2.4, 3.8, and 6.8 nm (Reprinted from Ni et al. (2016), Copyright 2016, with permission from WILEY-VCH Verlag GmbH & Co. KGaA, Weinheim); PL energies (f) and PL intensities (g) of Si NCs with different ligands (Reprinted from Li Q et al. (2016), Copyright 2016, with permission from American Chemical Society); (h) PL spectra of Te-doped ZnSe NCs (Reprinted from Sonawane et al. (2011), Copyright 2011, with permission from IOP Publishing); (i) FTIR spectra of Si NCs with different B levels (Reprinted from Ni et al. (2016), Copyright 2016, with permission from WILEY-VCH Verlag GmbH & Co. KGaA, Weinheim)

$$E_g = E_g(\text{bulk})\left(1 + \frac{2d}{D}\right),$$

where E_g is the band-gap energy of the NC, E_g(bulk) is the band-gap energy of the bulk semiconductor, d is the diameter of an atom, and D is the diameter of the NC. The validity of this model can be supported by comparing the calculated values with the experimental results (Figs. 1b and 1c).

There are some other effects of size besides the influence on electronic and optical properties. Ni et al. (2016) reported that the localized surface plasmon resonance of boron-hyperdoped silicon NCs changes significantly with NC size changes, as shown in Fig. 1e.

In addition, recent research about the role that size plays in the change in the band gap of semiconductor NCs shows that the effect of the surface energy and elasticity on the band-gap change exhibits size dependence, revealing a new scenario of size effect (Yang FQ, 2021).

2.2 Ligand effect

The surface state of NCs is another significant influencing factor on electronic structures due to the high surface-volume ratio (Dohnalová et al., 2014; Boles et al., 2016). The abundant dangling bonds on the surface introduce new electronic states into the band gap (Liu XK et al., 2016). When the surface atoms bond with the ligands, dangling bonds are satisfied, which pulls up the occupied surface states and pulls down the unoccupied surface states (Fig. 1d) (Kagan et al., 2016).

The optical absorption of NCs comes from the transition of electrons between discrete electronic states. Owing to the quantum confinement effect, NCs typically exhibit strong optical resonance absorption and nearly monochromatic carrier recombination (Lv et al., 2020). By adjusting the number of dangling bonds on the surface, recombination can be significantly affected. Surface modification also plays an important role in the storage and application of NCs. It can avoid aggregation (Lv et al., 2020), tune the electronic state (Zhao SY et al., 2018b), and control the resistive states of NC films.

As noted earlier, undercoordinated surface atoms contribute to electronic states, altering the electronic and optical properties of NCs (Kagan et al., 2016). The lower-energy states can be used as dopants, while the deeper band trail and the middle gap states act as capture traps which help in rapid electron-hole recombination (Yang J et al., 2016). The charge transfer between NCs and ligands is a significant process for the application of NCs. As the most obvious example of ligands affecting the optical properties of NCs, ligands can affect the emission wavelength of NCs (Figs. 1f and 1g). Some research has shown that the energy of photoluminescence is related to the dipole moment of ligands. Higher polarity leads to a red shift in photoluminescence (So et al., 2018). The carrier mobility of NC films is also affected by the ligand. Generally, carrier mobilities decrease exponentially with an increasing ligand length (Liu Y et al., 2010). This is because carrier mobility is hindered by energy barriers created by the modification of ligands. This barrier increases as the ligand length increases (Lv et al., 2020). Further, chemical changes of ligands can change the resistive states of NC films (Collier et al., 1997). Surface modification offers approaches for the adjustment and optimization of devices based on NCs.

2.3 Doping effect

Doping is one of the most frequently used methods to tune the properties of NCs (Arduca and Perego, 2017). A substitutional impurity consisting of one or more valence electrons compared to those of the host material donates its electron(s) to the semiconductor (n-type doping), and an impurity with fewer valence electrons donates holes (p-type doping) (Norris et al., 2008). Doping can influence the electronic structure of a NC and change its band gap, causing a series of variations in absorption and emission. Fig. 1h shows the photoluminescence of ZnSe NCs with different doping concentrations of Te (Sonawane et al., 2011). The change in band gap leads to a photoluminescence peak shift, and with the introduction of new electronic states, some new peaks appear (in this example, the peak is at 522 nm). The existence of impurity states also has an effect on carrier transport and surface activity, which can be seen from the intensity of absorption or emission. Moreover, one study shows that localized surface plasmon resonance depends on the doping concentration when the NC size has been determined (Fig. 1i) (Ni et al., 2016).

3 Synaptic devices based on NC films

NCs need to be integrated into NC solids (generally thin films) for device application. Traditional approaches to NC film formation include drop casting (Talapin and Murray, 2005), spin casting (Coe et al., 2002; Gur et al., 2005), dip coating (Talgorn et al., 2011), Langmuir−Blodgett deposition, and doctor blading.

Yang J et al. (2016) compared these methods and summarized their equipment, waste, film thickness, uniformity, and ability for continuous process (Table 1).

Drop casting is the simplest method with no need for controlling the environment, but it has the worst film uniformity and a poor controllability of film thickness.

Spin casting is more widely used and is more likely to form a film with high uniformity. The film quality and thickness of spin casting depend on the solvent, NC concentration, as well as rotational speed.

Dip coating is carried out in solution, where the NC film is deposited on substrates. This method can be used for roll-to-roll continuous process and is well-established in the industry. The uniformity of films formed by this method is not optimal owing to process-related edge effects, but it can be overcome by scaling-up.

In Langmuir−Blodgett deposition, the NC layer is formed on a liquid surface, and is then transferred to a target substrate. The film is fabricated by the successive deposition of individual NC layers, and thus the film obtained by this method can have a high film quality and an adjustable thickness in a large range (Yang J et al., 2016).

Doctor blading is another method compatible with industry. Its name comes from its signature scraping operation. The thickness of films depends on the distance between the blade and the substrate, which determines that the NC film cannot be as thin as a layer of a few atoms.

With recent advances in precise control technologies, patterning methods for the formation of NC films have emerged, been developed, and have gradually matured. Inkjet printing is relatively mature and is often used in the preparation of NC films with RGB patterns (Jiang et al., 2016). Tiny droplets dissolved with NCs are accelerated by an electric field and hit the substrate. The two main advantages of this method are low material loss (Service, 2004) and an adaptation to printing large and complex patterns (Yu et al., 2012). However, due to the inhomogeneous evaporation of solvent, NCs may cluster at the edge of the droplet—called the “coffee ring effect” (Deegan et al., 1997). This issue is typically solved by the addition of another solvent with a higher boiling point and a lower surface tension to form a surface tension gradient to prevent solvent flow during evaporation (Hu H and Larson, 2005). Jiang et al. (2016) used a substrate with high surface free energy (polyetherimide-modified ZnO nanopartical layer) to enhance the evaporation rate of mixed solvents. They successfully obtained a NC film without coffee rings.

3.1 Synaptic devices based on common NC films

With a tunable band gap and remarkable electronic and optical properties, semiconductor NCs have been widely used in the fabrication of synaptic devices. Si is one of the most frequently studied elements for semiconductors, and its NCs have also been applied to synaptic devices in recent years. Resistive switches (also called memristors) belonging to two-terminal devices are a common type of synaptic devices, in

Table 1 Comparison of the film-forming techniques for colloidal NCs

Type	Equipment	Waste	Film thickness	Uniformity	Roll-to-roll continuous process
Drop casting	None	Little	Monolayer to several micrometers	Very low	No
Spin casting	Spin-coater	Significant	Monolayer to hundreds of nanometers	High	No
Dip coating	Dip-coater	Little	Monolayer	Moderate	Yes
Langmuir–Blodgett deposition	Langmuir–Blodgett through	Little	Monolayer to several layers	Extremely high within monolayer	Yes
Doctor blading	Blade	None	Several micrometers	Moderate	Yes

Reprinted from Yang J et al. (2016), Copyright 2015, with permission from WILEY-VCH Verlag GmbH & Co. KGaA, Weinheim

which Si NCs are largely applied. Kawauchi et al. (2019) demonstrated an electrically stimulated synaptic resistive switch with a resistance change of about 10^3. Iconic synaptic functions like short-term plasticity (STP), long-term plasticity (LTP), and simulated spike-timing-dependent plasticity (STDP) were all realized in this memristor. The Si NC film they used consists of natively oxidized Si NCs with a nonstoichiometric, amorphous SiO_x shell. The relationship between the resistive switch and the electrode area has been investigated, and the formation mechanism of the oxygen vacancy filament has been interpreted.

In Kawauchi et al. (2019)'s work, several Al electrodes with different areas were formed on the Si NC film by evaporation. A typical bipolar resistive switch with a 0.79 mm^2 Al electrode is shown in Fig. 2a, a cycle-to-cycle variation of switching is shown in Fig. 2b, and a device-to-device variation in four devices is shown in Fig. 2c. Notice that the forming voltage of this device is free. The reproducibility of switching behavior with an electrode area of 0.25 mm^2 is shown in Fig. 2d, and the set/reset voltage within 30 cycles is shown in Fig. 2e. In Fig. 2f, the resistance normalized by electrode area (R_{square}) in the high resistance state (HRS) and the low resistance state (LRS) is plotted, which indicates that the change of device resistance cannot be explained simply. By using set voltage pulses, the device current can be conducted. The resistive switching model in Si NC films is shown in Fig. 2g. In HRS (state i), there is no conductive path formed in the SiO_x shell. Under a large electric field, oxygen ions diffuse, and a collection region of oxygen vacancies is formed (state ii). Then, a conductive filament is formed and the resistance state turns to LRS (state iii). A reverse electric field with enough strength can force the film back to HRS. By evaluating the activation energy of the conductive filament formation, we find that the switching time for the set operation is limited by a migration of oxygen interstitial ions.

Owing to the absorption and emission properties of NCs, photoelectric conversion devices based on NCs have been widely studied in recent years. Tan et al. (2018) fabricated an optical input optoelectronic synapse (Fig. 3a) with a broad spectral region from ultraviolet to near-infrared, the energy consumption of which is only about 0.7 pJ for a spike duration of 0.1 s. Their device realized STDP (Fig. 3b) and showed the dependence of the asymmetric degree of synaptic weight change on incident laser wavelength (Fig. 3c). A model of the electronic structure of Si NCs is built in Fig. 3d, showing the carrier behavior after optical absorption. The photogenerated electrons can be trapped by deep energy levels introduced by dangling bonds and slowly released to the conduction band, which leads to photocurrent decay.

In recent years, green electronics have garnered much attention due to their environment friendliness. Hussain et al. (2022) reported a new idea of using Ag nanoparticles and cellulose nanocrystal (CNC) as the active layer of memristors (shown in Fig. 3e), through which a high on/off ratio ($\approx 10^4$) and ultralow set/reset voltage ($\approx$0.2 V) were realized. The switch of the resistive state was realized by controlling the formation and fracture of conductive Ag filaments.

In comparison with two-terminal devices, three-terminal devices have a more complex structure and benefit from better stability as well as from controllability of testing parameters (Dai et al., 2019). Yin et al. (2019) fabricated optoelectronic synaptic devices based on Si NCs that not only implemented aversion learning and logic functions, but also realized the recognition of handwritten digits with a currency of around 94%. Due to the ability of gate control, it is clearly simpler to implement logic functions than it is in the two-terminal synaptic devices mentioned above. An electrical spike and an optical spike are regarded as two separate input signals. For the "AND" operation, an electrical spike with a positive V_g is applied, while for the "OR" operation, a negative V_g is used. The implementations of "AND"/"OR" operations and taste-aversion learning are shown in Figs. 3f and 3g, respectively. A situation in which an alcohol addict is treated for abstinence is imagined, in which the excitatory electrical stimulation and the inhibitory optical stimulation are used to mimic the effect of alcohol and emetine-induced emesis. In Fig. 3g, an excitatory postsynaptic current (EPSC) and an inhibitory postsynaptic current (IPSC) represent the current level of craving and aversion, respectively. After the aversion-learning process (the coexistence of excitatory electrical stimulation and inhibitory optical stimulation), the current level is restricted to an aversion state, though the excitatory stimulation of alcohol is still ongoing.

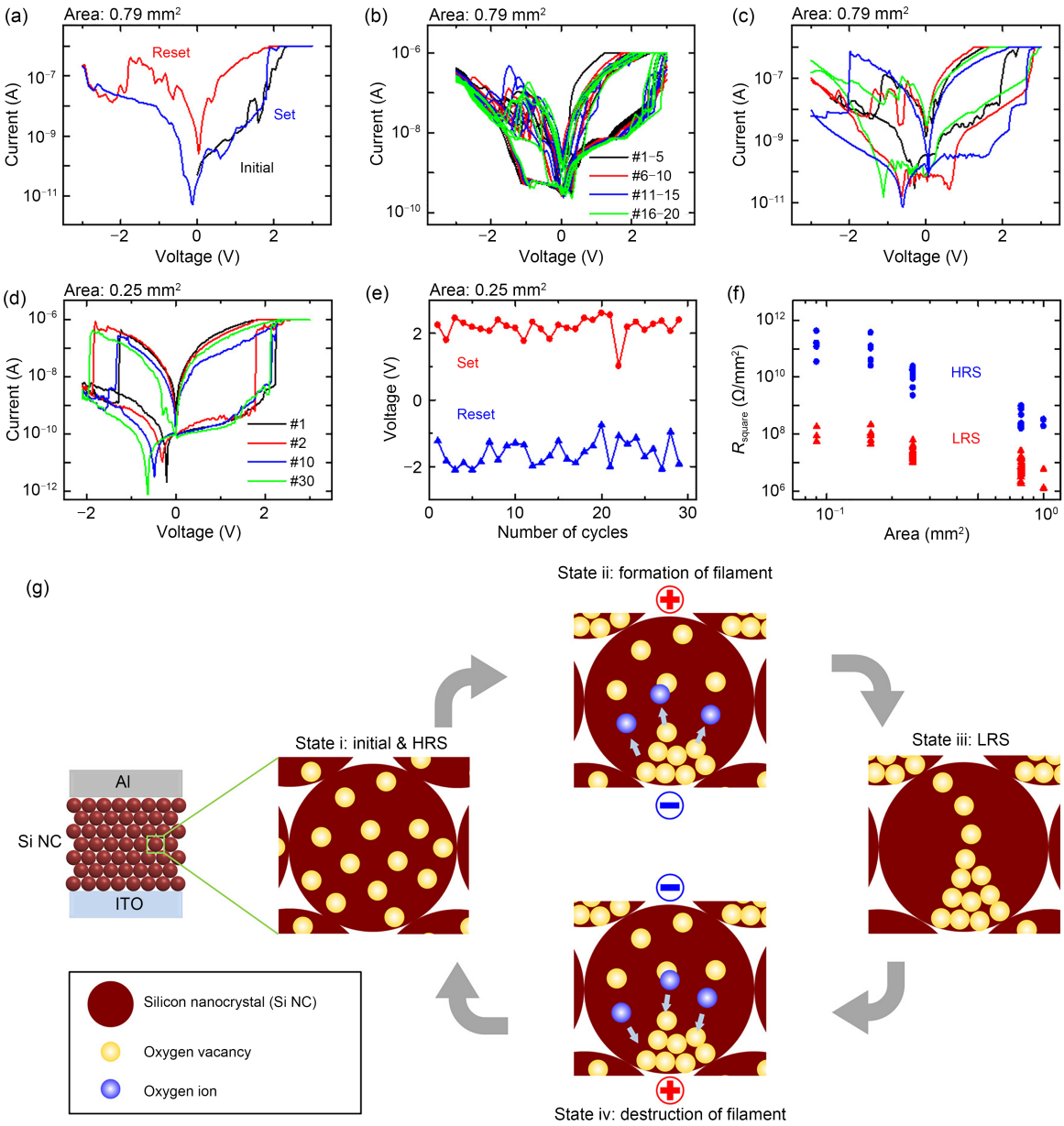

Fig. 2 (a) A typical bipolar resistive switch with an electrode area of 0.79 mm²; (b) cycle-to-cycle variation of switching with an electrode area of 0.79 mm²; (c) device-to-device variation of switching in four devices with an electrode area of 0.79 mm²; (d) reproducibility of a resistive switch with an electrode size of 0.25 mm²; (e) set and reset voltages within 30 cycles with an electrode area of 0.25 mm²; (f) dependence of R_{square} on the electrode area in the high resistance state (HRS) and low resistance state (LRS); (g) schematic illustration of the formation and destruction of oxygen vacancy conductive filaments. Reprinted from Kawauchi et al. (2019), Copyright 2019, with permission from American Chemical Society

3.2 Synaptic devices based on core-shell NC films

The term "core-shell NCs" denotes concentric multilayer semiconductor NCs, which may have many different shapes (Fig. 4a) (Chaudhuri and Paria, 2012). Because of the band-gap difference between the core and the shell (for example in Fig. 4b), a carrier undergoes a periodic potential just as in a situation in a quantum well. Hence, core-shell NCs are also called quantum-well NCs.

Due to their unique role in charge trapping, core-shell NCs are promising materials for the fabrication of synaptic devices. They have been used in memory devices as early as 2007 (Li FS et al., 2007). Optical programming (Chiu et al., 2009) was soon realized

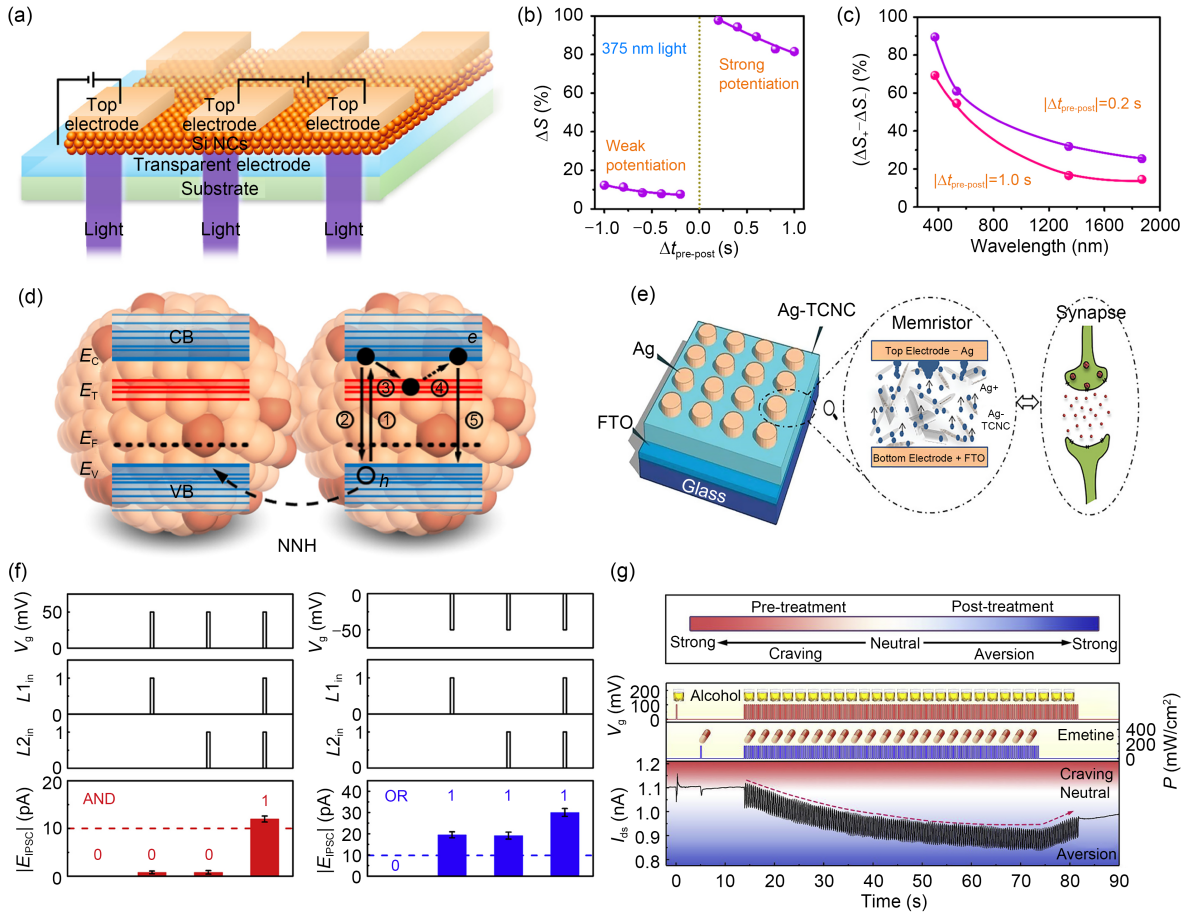

Fig. 3 (a) Schematic of the Si-based synaptic devices; (b) dependence of STDP-introduced synaptic-weight change on the interval of laser spikes; (c) relationship between the asymmetric degree of Δ*S* and laser wavelength; (d) a model of electronic structure and carrier behavior in Si NCs; (e) schematic of the structure of the bio-memristor; (f) implementation of logic functions of the "AND" and "OR" gates; (g) implementation of taste-aversion learning. (a)–(d) are reprinted from Tan et al. (2018), Copyright 2018, with permission from Elsevier Ltd.; (e) is reprinted from Hussain et al. (2022), Copyright 2021, with permission from Wiley-VCH GmbH; (f) and (g) are reprinted from Yin et al. (2019), Copyright 2019, with permission from Elsevier Ltd. STDP: spike-timing-dependent plasticity; NC: nanocrystal

with memory devices based on core-shell NCs. Yan CY et al. (2019) fabricated a nonvolatile memory using ZnSe@ZnS core-shell NCs and studied the role of the ligand in charge transport. In many cases, core-shell NCs are combined with organic semiconductors to form a synaptic device—something that will be discussed later.

4 Synaptic devices based on NC heterojunction

4.1 Heterojunction devices of NCs with perovskite

The combination of NCs with other materials may add some more complex functions to devices (Wang Y et al., 2022). Perovskite possesses some beneficial properties such as high carrier mobility and high luminous efficiency, although its stability has long been a focus of criticism. Zhu YY et al. (2020) used organometal halide perovskite with excellent optical absorbing properties to realize an improvement in optical sensitivity and a decrease in energy consumption. Huang et al. (2020) fabricated a photoelectric conversion synaptic device with a laminated structure of organometal halide perovskite and Si NCs. One of the most significant properties of their device is that it works only with optical inputs, and there is no need for electricity (zero-power). Some important synaptic functionalities such as paired pulse facilitation (PPF), STDP, spike-number-dependent

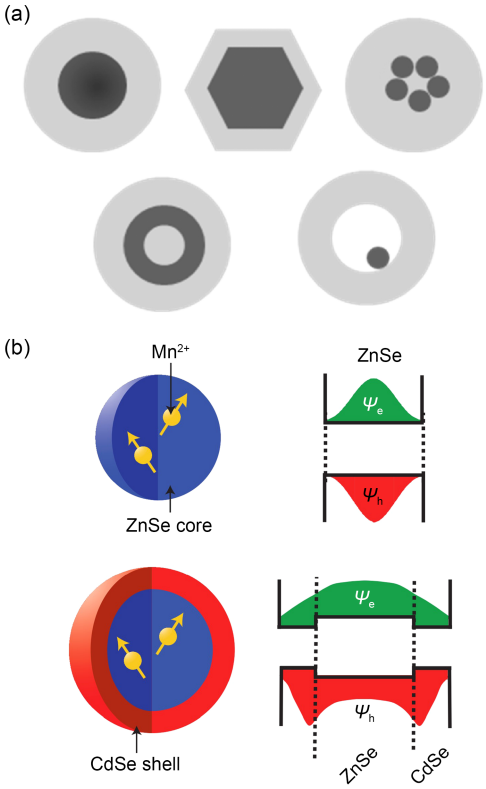

Fig. 4 (a) Core-shell NCs with different shapes (Reprinted from Chaudhuri and Paria (2012), Copyright 2012, with permission from American Chemical Society); (b) Mn^{2+}-doped cores of ZnSe overcoated with CdSe shells (Reprinted from Bussian et al. (2009), Copyright 2008, with permission from Nature Publishing Group)

plasticity (SNDP), and spike-rate-dependent plasticity (SRDP) have also been realized, based on which their device can be applied to image sharpening. The device was fabricated with a multilayer structure (Fig. 5a) of indium tin oxide (ITO)/phenyl-C61-butyric acid methyl ester (PCMB)/$MAPbI_3$:Si NCs/2, 20, 7, 70-tetrakis[N, N-di(4-methoxyphenyl) amino]-9, 90-spirobifluorene (Spiro-OMeTAD)/Au on glass. The EPSC of this device was induced by a laser with a wavelength of 375 nm, based on the hybrid structure of $MAPbI_3$ and Si NCs. The Si NCs used in Huang et al. (2020) were heavily doped with boron (B), leading to a low Fermi level near the peak valance band. $MAPbI_3$ has a Fermi level near the middle of the band gap (Wang Q et al., 2014). Different Fermi levels cause the transferring of carriers and the formation of a built-in electric field, under the influence of which photogenerated carriers were separated and transferred. Figs. 5b and 5c show the PPF effect and the relationship between the PPF index and time interval, respectively, which can indicate the plasticity of the devices (Debanne et al., 1996; Kim et al., 2013). Fig. 5d shows EPSCs stimulated by laser with a different spike number, which can indicate the SNDP effect of the device. SRDP was also realized by applying optical spikes with different frequencies (Fig. 5e), showing long-term synaptic properties (D'amour and Froemke, 2015; Wang ZQ et al., 2020). For 50 optical spikes, the ratio of the EPSC evoked by the last spike to the first EPSC was defined as "Gain." The relationship between "Gain" and the frequency of spikes is shown in Fig. 5f.

Huang et al. (2020) fitted this relationship with a high-pass filter function and found that their device can be used as a high-pass filter with a cutoff frequency of 4.8 Hz. They used their device to sharpen the flower image shown in Fig. 5g, and the sharpened image they finally acquired is shown in Fig. 5h. Compared to standard image processing, which is obtained using a cutoff frequency larger than 4.8 Hz (Fig. 5i), the sharpened image shows a significant improvement.

Compared to the structure of NCs dispersed in perovskite, the heterostructure of perovskite NCs with other materials is better (which will be introduced in Sections 4.2 and 4.3). Though the application of perovskite improved performance, the devices are plagued by poor stability and become a bottleneck in large-scale applications. Even marginal heat accumulation or transient air exposure may degrade a device's performance—which can be attributed to a degradation-induced interface state (Ma HL et al., 2018). In addition to conventional means such as atmosphere and temperature control, new methods—for example introducing light irradiation into the electroforming process of perovskite-based memristors to boost their reliability (Zhao XN et al., 2020)—need to be developed.

4.2 Heterojunction devices of NCs with organic semiconductors

In similar work, Zhao SY et al. (2018a) fabricated optical-output synaptic devices based on Si NCs with a multilayer structure of ITO/ZnO/Si NCs/4, 4'-bis(carbazol-9-yl) biphenyl (CBP)/MoO_3/Au. These devices have a red emission of about 740 nm,

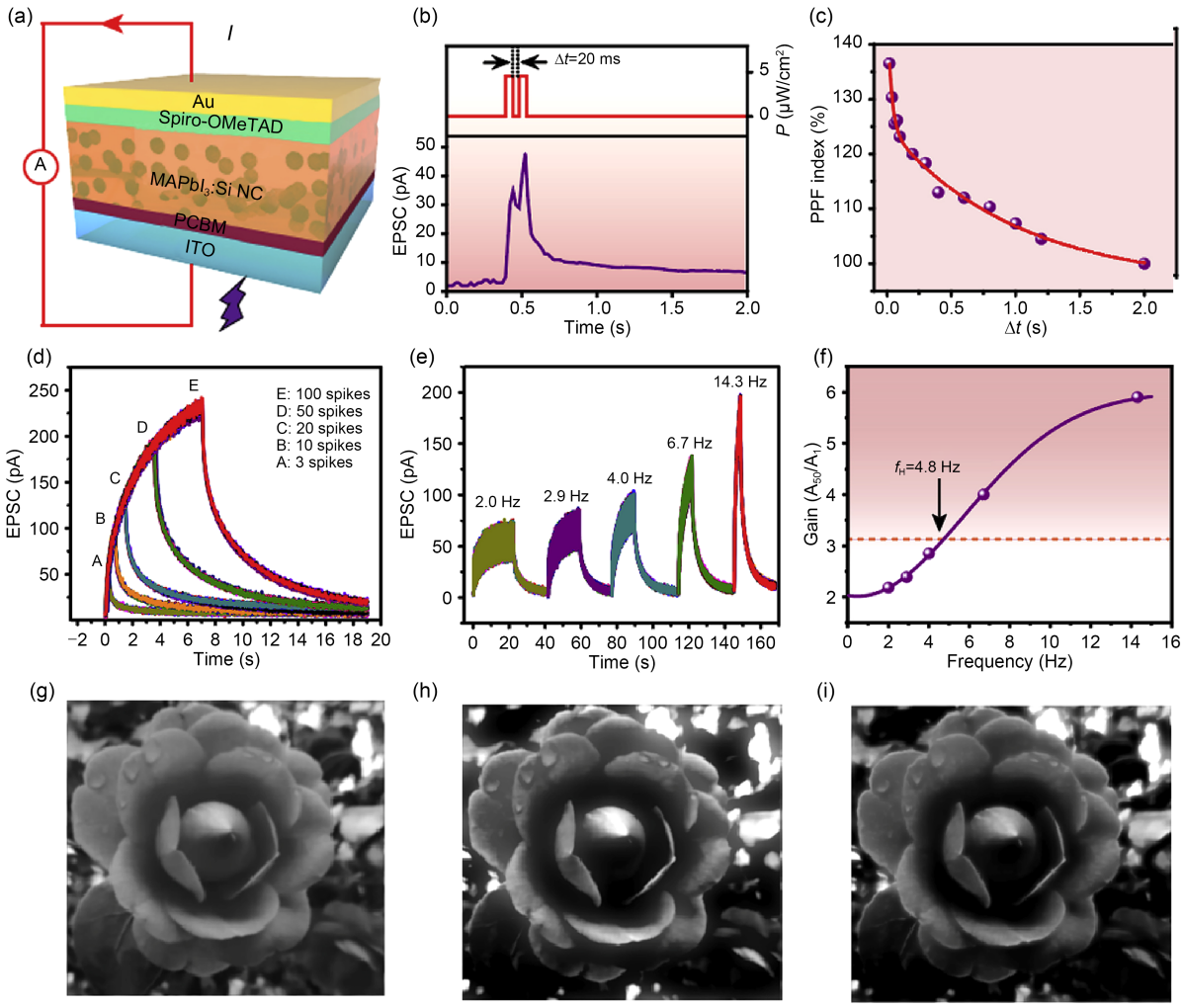

Fig. 5 (a) Device structure; (b) paired pulse facilitation (PPF) effect of the device; (c) dependence of the PPF index on the time interval of optical stimulation; (d) excitatory postsynaptic current (EPSC) stimulated by spikes with different numbers; (e) EPSC stimulated by spikes with a different frequency; (f) relationship between the Gain and spike frequency; (g) original image of a flower; (h) image sharpened with a cutoff frequency of 4.8 Hz; (i) image sharpened with a cutoff frequency of 19 Hz. Reprinted from Huang et al. (2020), Copyright 2020, with permission from Elsevier Ltd.

exhibiting many important synaptic functionalities such as PPF, STDP, as well as the transition from STP to LTP, and can be used to realize logic functions.

The geometry of the devices is shown in Fig. 6a. Two devices are intercoupled with a symmetric configuration (Fig. 6b). E_1 and E_2 are input terminals and L is the output terminal. The schematics of the logic functions are shown in Figs. 6c and 6d. Zhao SY et al. (2018a) defined a low voltage of 0 V as input "0," and input "1" is defined as high as about 6 V. The output signal is defined with a threshold value of 1 μW. When the value is higher than the threshold, it is defined as "1," and when the value is lower than the threshold, it is defined as "0." So, according to the output current, "AND" and "OR" gates are realized in Fig. 6e. The realization of "NAND" and "NOR" is similar, but their output threshold is defined with a resistance of 0.1 Ω. The histograms of the logic functions of "NAND" and "NOR" are shown in Fig. 6f.

In addition to the realization of synaptic functions, storage stability plays a role in the evaluation of synaptic devices. Wang Y et al. (2018) reported a $CsPbBr_3$ perovskite–nanocrystal (PQDs) based photonic flash memory (Fig. 7a). The device realized basic synaptic functions and also showed important optically programmable and electrically erasable characteristics of nonvolatile storage. The light-programming

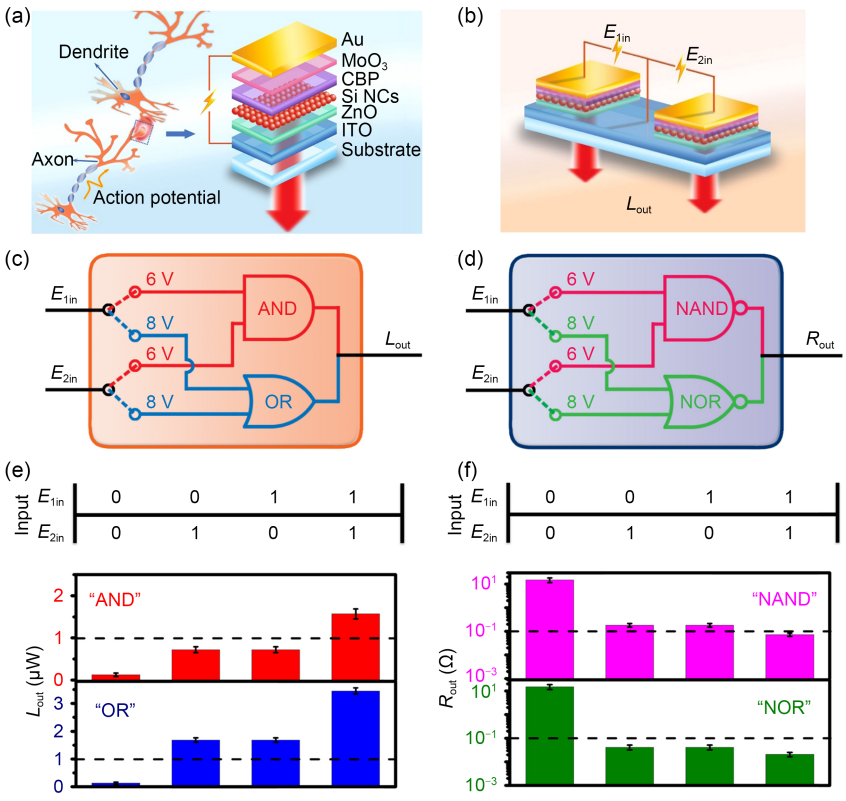

Fig. 6 (a) Geometry of the electroluminescent devices based on NCs; (b) schematic of two devices intercoupled with a symmetric configuration; schematic operation diagrams of "AND" and "OR" gates (c) and "NAND" and "NOR" gates (d); histograms of the logic functions of "AND" and "OR" (e) and "NAND" and "NOR" (f). Reprinted from Zhao SY et al. (2018a), Copyright 2018, with permission from Elsevier Ltd.

operation and electric erasing operation are shown in Fig. 7b. During the programming operation, photogenerated holes escape to pentacene and become carriers owing to the band-bending caused by the application of negative gate bias, while photogenerated electrons are trapped in the NC layer. After the removal of light, the carrier distribution is restored by applying a positive bias. In 2021, a similar P3HT/PQDs-heterojunction-based synaptic device with photo writing and electric erasing functions showing ultrafast response was reported (Chen et al., 2021). This synapse can respond to an extremely short illumination of 1 ms with a lowest energy consumption of 3×10^{-17} J. Phototransistors based on perovskite NCs have attracted many researchers recently. These devices are often sensitive and have high responsivity. Hao et al. (2020) reported a photonic synaptic transistor based on organic semiconductor poly[2, 5-(2-octyldodecyl)-3, 6-diketopyrrolopyrrole-alt-5, 5-(2, 5-di(thien-2-yl) thieno [3, 2-b]thiophene)] (DPPDTT) and perovskite $CsPbBr_3$ NCs. The device exhibits high photo-sensitivity and shows an obvious synaptic response even under an ultralow operation voltage of −0.0005 V. Wang K et al. (2019) reported a new kind of light-stimulated synaptic transistor (LSST) based on inorganic halide perovskite NCs and organic semiconductors. The hybrid structure leads to a high separation efficiency of charge, improving photoresponsivity by about three orders of magnitude higher compared to that of devices based on pure NCs.

Li EL et al. (2019) reported an all-inorganic synaptic transistor based on L-type, ligand-modified, $CsPbBr_3$ perovskite NCs, which possibly confirms the feasibility of the modulation of synaptic plasticity via temperature control and waveform modulation of the excitation wave. A schematic of the device structure is shown in Fig. 7c. Fig. 7d shows the channel currents excited by different pulse widths at different temperatures. The synaptic weight is enhanced with the increase in temperature. The temperature-dependent EPSC decays after removing the excitation pulse are presented in Fig. 7e. This phenomenon

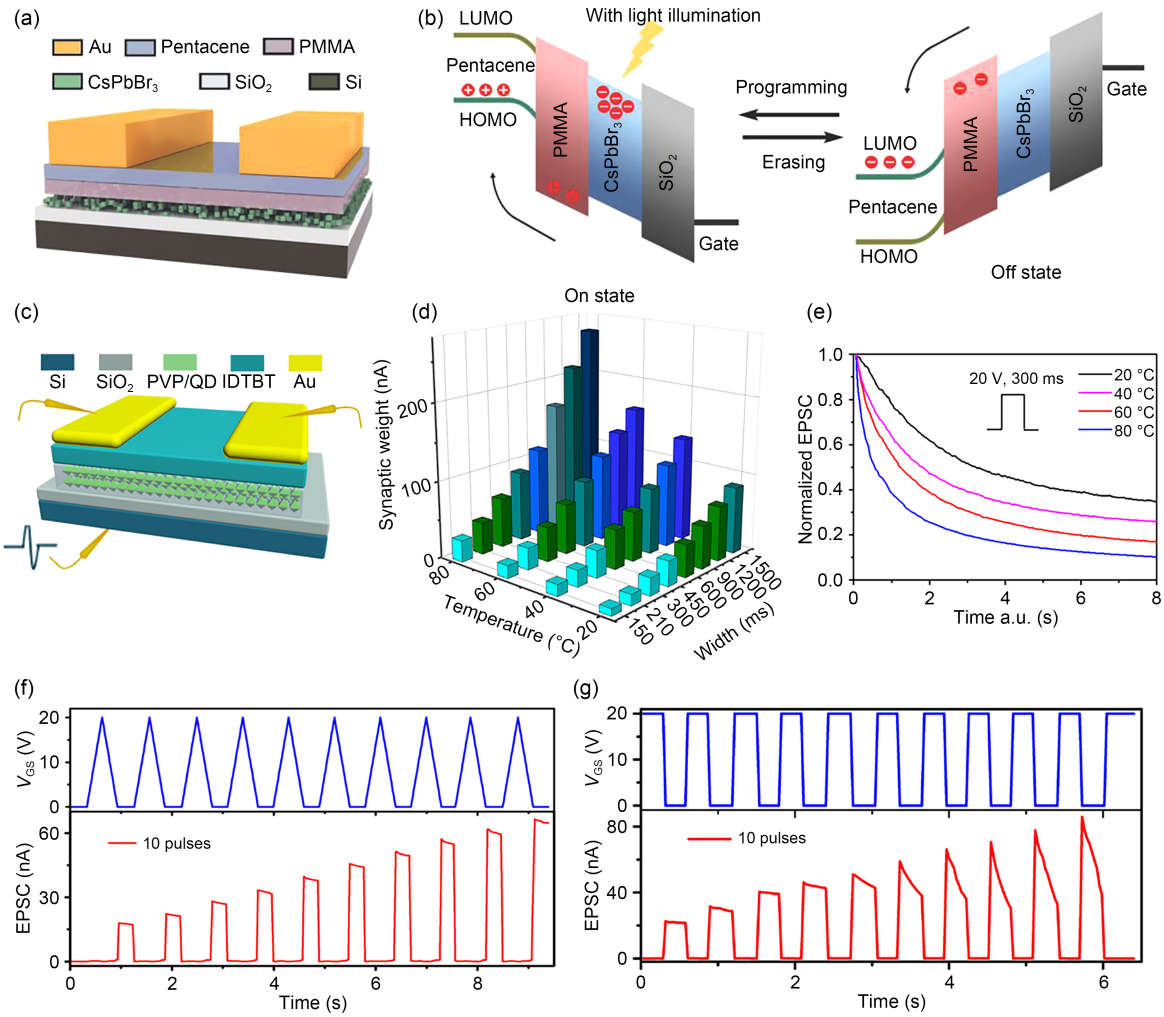

Fig. 7 (a) Schematic of photonic memory; (b) optical programming operation and electric erasing operation; (c) schematic of the temperature-controlled device; (d) synaptic weight as a function of pulse width under diverse temperatures; (e) EPSC decays after removing the excitation pulse under four temperature levels; EPSC stimulated by 10 consecutive pulses of triangular waves (f) and square waves (g). (a) and (b) are reprinted from Wang Y et al. (2018), Copyright 2018, with permission from WILEY-VCH Verlag GmbH & Co. KGaA, Weinheim; (c)–(g) are reprinted from Li EL et al. (2019), Copyright 2019, with permission from American Chemical Society

originates from a stronger intrinsic excitation as well as from a higher carrier mobility induced by heating, which accelerates the de-trapping process. The effect of high temperature boosts the basic current level, accelerating the learning process and enhancing the relaxation process. Figs. 7f and 7g show the EPSC realized by 10 identical triangular pulses and by 10 consecutive square pulses, respectively. The triangular waves and square waves have the same integral area, and the parameters of the triangular wave are set to 20 V, 600 ms of base, and 300 ms of interval. As shown in Fig. 7, the current stimulated by the square waves was larger than that stimulated by triangular waves. This is because the low-voltage sections—which can only slightly influence the amplitude of current owing to the shielding effect of insulating and semiconductor layers—are much more in triangular waves than in square waves. The decay curves can be fitted by the power function:

$$y=a+b\times t^{-m},$$

where a and b are constants, t is the time, and m is the decay rate of memory retention. The decay rate of triangular waves is smaller than that of square waves, indicating that the retention time of memory formed

by triangular waves is longer than that formed by square waves.

In recent years, more attention has been paid to flexible electronics. Carbon and its oxide NCs exhibit impressive properties such as good biocompatibility, low toxicity, and aqueous solubility, which have potential for biological applications such as flexible synapses (Li XM et al., 2015). The large-scale application of carbon NC materials is also a building block for the development of wearable electronics. Wang TY et al. (2020) and Zeng et al. (2021) fabricated a flexible and transparent synaptic device based on polyvinylpyrrolidone (PVP)/N-doped carbon NC (NCNC) nanocomposites. It can realize general memristive switching, for which there is a critical need in biorealism applications. This feature is realized via modulating the number of conductive paths (CPs) by changing the NCNC concentration. The memristive behavior of the synapse can also be changed via regulating the doping concentration of NCNCs, through which the transition from HRS to LRS can be realized.

The structure of the device is shown in Fig. 8a. Fig. 8b shows the flexibility and transparency of the device. The state in which devices can show the switch of the resistance state (from LRS to HRS, or the converse) is called the digital-type resistance state (known as D-RS). Figs. 8c and 8d give the D-RS and analog-type RS (A-RS) of the device, respectively. There is no RS behavior without inserting NCNCs into PVP film. When the concentration of NCNCs reached 10-weight percent, a typical D-RS behavior occurs. Once the concentration of NCNCs increases to 30-weight percent, the set and forming voltage decreases substantially, and the D-RS turns to A-RS when the concentration of NCNCs increases to 40-weight percent. The concentration-induced change in resistance can be explained by the difference in CPs. A low NCNC concentration leads to a dominant CP (Fig. 8e), which corresponds to an instant change from HRS to LRS. A high NCNC concentration can afford multiple CPs (Fig. 8f), and thus the device resistance can be affected by the NCNC concentration.

The establishment of a photonic neural network without a physical connection is a meaningful topic because the information transfer between two synaptic

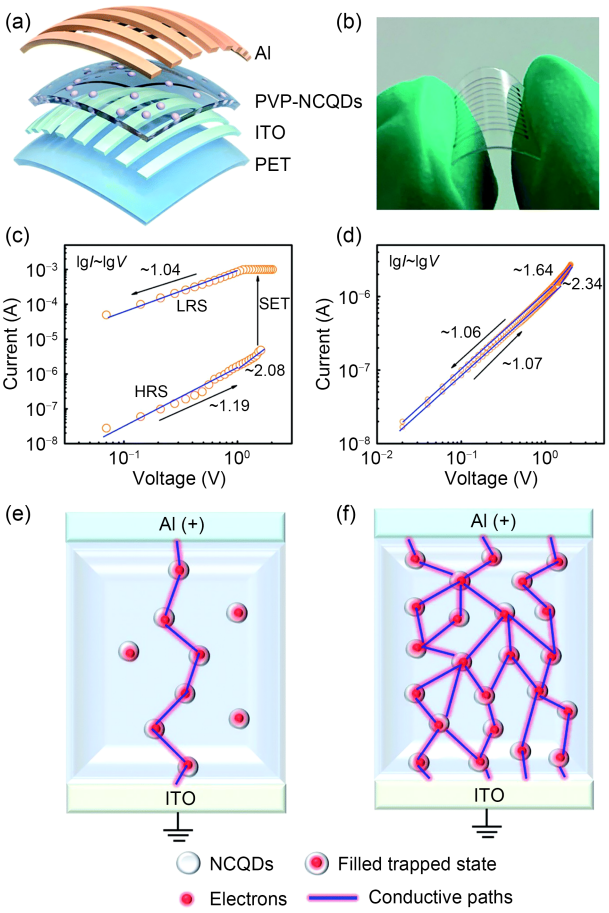

Fig. 8 (a) Structure of polyvinylpyrrolidone (PVP)/N-doped carbon NC synaptic devices; (b) photo of the flexible device on a PET substrate; (c) D-RS of the device under a low NCNC concentration; (d) A-RS of the device under a high NCNC concentration; schematic of the mechanism of D-RS (e) and A-RS (f). Reprinted from Zeng et al. (2021), Copyright 2021, with permission from the authors, licensed under CC BY 3.0

devices needs to be rapid with high fidelity. Compared with electrical signals, optical signals provide benefits such as high bandwidth (Lee WCA et al., 2016), low energy consumption (He WX et al., 2019), and low crosstalk (Zhu LQ et al., 2015; Sun et al., 2021a). Owing to a low loss of near-infrared (NIR) light during transmission through most technologically important materials, synaptic devices with luminescence in the NIR region warrant more research. A problem that cannot be ignored is that the hole mobility of hole-transport materials is often much lower than that of the electron mobility of electron-transport materials in light-emitting devices, leading to an imbalance of carrier injection. Zhao SY et al. (2019)

reported improved NIR light-emitting diodes and presented successful simulating of the synaptic function. The light-emitting device has a multilayer structure of Ag/ZnO/Si-QDs/PFN/poly(3-hexylthiophene) (P3HT)/poly(3, 4-ethylenedioxythiophene)/polystyrene sulfonate (PEDOT:PSS)/ITO/glass (Fig. 9a), and P3HT was used as the hole-transport layer. P3HT has negligible NIR absorption and high hole mobility, mitigating the imbalance of carrier injection. The addition of poly[9, 9-bis(3'-(N, N-dimethylamino) propyl)-2, 7-flourene]-alt-2, 7-(9, 9-dioctylfluorene)] (PFN) between Si NCs and the P3HT layer further enhances the performance by mitigating electron leakage from the Si NCs. Zhao SY et al. (2019) showed the possibility of applying light as a transmission signal in integrated devices.

It is worth noting that the establishing of a compact artificial neural network is now limited by the input-output matching of different devices. The development of synaptic devices with optical output is not as rapid as that of devices with electrical output. In 2021, an artificial efferent neural system, in which the optical output signal of the pre-memristor can be used directly as the input signal of the post-memristor, was established by Zhu YB et al. (2021). It is recognized as the first realization of an optical output function in synaptic devices. The neural system comprises a kind of light-emitting memristor which combines the functions of light-receiving, light-emitting, and optoelectronic synapses. The light-emitting memristor consists of ITO/PEDOS:PSS/copper(I) thiocyanate (CuSCN)/poly(9, 9-dioctylfluorene-co-N-(4-butylphenyl)diphenylamine) (TFB)/CdSe@ZnS core-shell NCs/ZnO nanoparticles/Ag, as shown in Fig. 9b. It contains a light-emitting layer composed of blue CdSe@ZnS NCs, a hole transport layer of CuSCN/TFB, and an electron transport layer of ZnO nanoparticles (Zhu YB et al., 2021). The optoelectronic artificial nerve is shown in Fig. 9c, where the pre- and post-synaptic membranes are simulated by light-emitting memristors. The signal transmission is based on optical communication without the participation of external light sources. As shown in Fig. 9c, this neural system can implement one-to-many transmission and dynamically adjustable transmissions due to a signal transmission mode based on light emission and light absorption. The impressive synapse-like optical output is due to hole collection and the release of the CuSCN layer under blue-light stimulation (Fig. 9d).

The neural system established by Zhu YB et al. (2021) provides a successful and important example of how artificial neural networks can be constructed without external exciting sources, which removes the limitations arising from the physical medium. To date, there have been few reports of synaptic devices with optical output. More studies about synaptic devices with other color output and reasonable integrating mode are still needed.

Memories based on the heterojunction of NCs and organic semiconductors have been developed rapidly. Hu H et al. (2021) reported a pentacene-based organic transistor with InP@ZnS core-shell NCs integrated, achieving a fast response (10 μs), a large memory window (42 V), and a retention time as long as 4×10^4 s. In the same year, He LH et al. (2021) combined ferroelectric poly(vinylidene fluoride-co-trifluoroethylene) (P(VDF-TrFE)) with core-shell CdSe@ZnS NCs in an organic thin-film transistor that exhibits an excellent switch ratio ($\approx10^5$) and excellent retention (10^4 s).

4.3 Heterojunction devices of NCs with two-dimensional (2D) materials

Synaptic devices based on Si NCs have been widely researched. The energy consumption of these devices has been reduced to a significantly low level. Ni et al. (2018) fabricated an optoelectronic synaptic device with a hybrid structure of Si NCs and 2D WSe_2. The device shows a broadband photo-response from the ultraviolet to the near-infrared and presents a low energy consumption of about 75 fJ.

In contrast, three-terminal synaptic devices based on transition metal dichalcogenide NCs have rarely been reported. Sun et al. (2021b) reported an optoelectronic synaptic transistor based on a MoS_2/NCs heterostructure with optically modulated plasticity and erasable features.

Fig. 10a shows the change of light-induced post-synaptic current (PSC) under constant gate stimulation. Sun et al. (2021b) believed that this phenomenon was the result of the different responses of the device with applied voltage spikes under different light conditions. Fig. 10b shows the erasing operation on long-term depression. A large voltage is applied to the gate at 16 s and the EPSC is immediately gone.

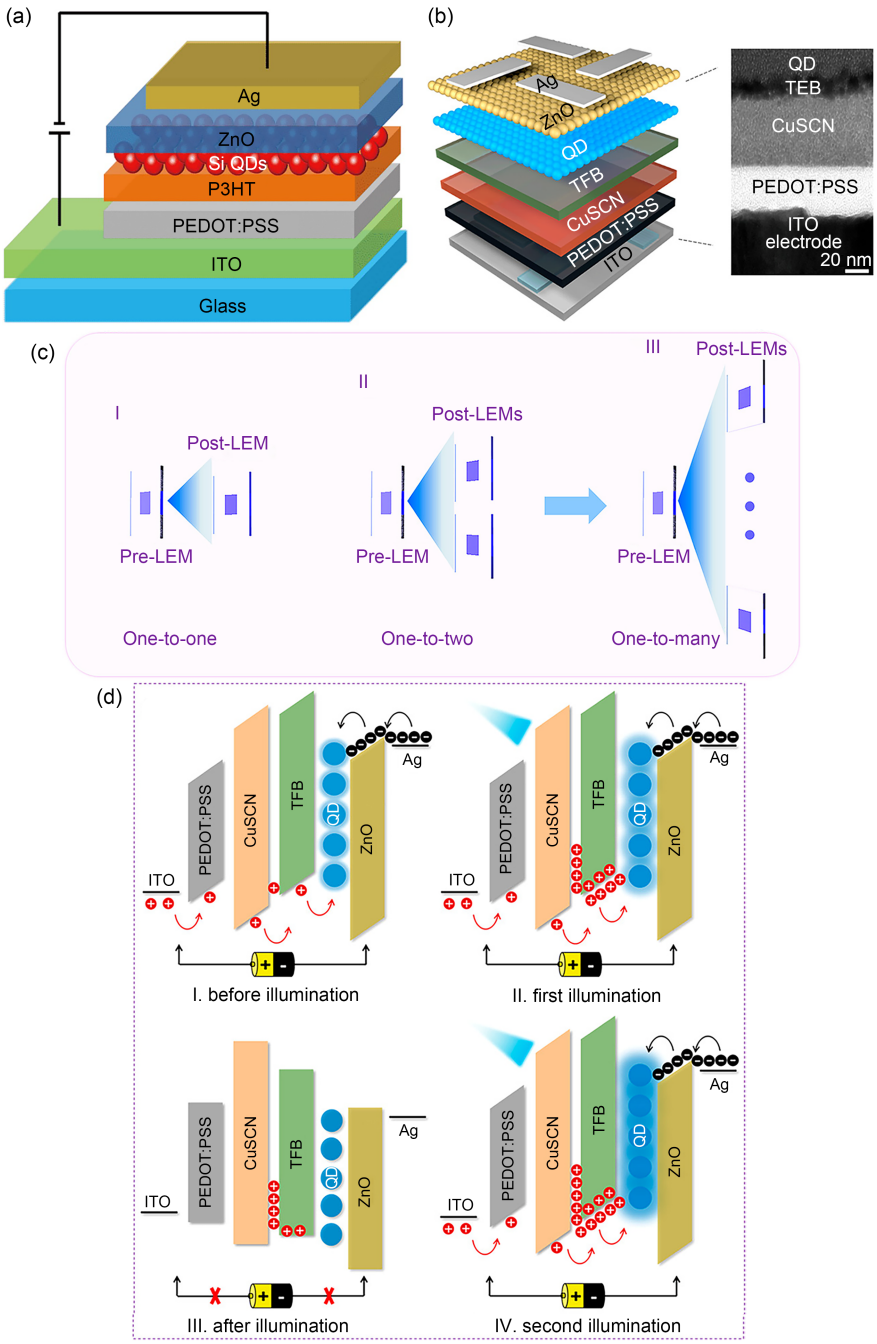

Fig. 9 (a) Schematic of an NIR light-emitting synaptic device with an organic transport layer of P3HT; (b) schematic of the light-emitting memristor; (c) schematic showing the dynamic adjustable information transmission; (d) working mechanisms of a single synaptic device. (a) is reprinted from Zhao SY et al. (2019), Copyright 2019, with permission from Science China Press and Springer-Verlag GmbH Germany, part of Springer Nature; (b)–(d) are reprinted from Zhu YB et al. (2021), Copyright 2021, with permission from American Chemical Society

Due to the flexibility of 2D materials, the heterostructure of NCs and 2D materials has also been used in flexible devices. As a representative work, Hou et al. (2021) fabricated an optical synapse based on a pyrenyl graphdiyne (Pyr-GDY)/graphene (Gr)/PbS NC heterostructure (Fig. 10c). The main innovation of this work is two-light regulation (Fig. 10d). Light of 980 nm can excite only the electrons in PbS NCs, causing a transfer of photogenerated holes from PbS NCs to Gr. So, the conductivity of Gr decreases

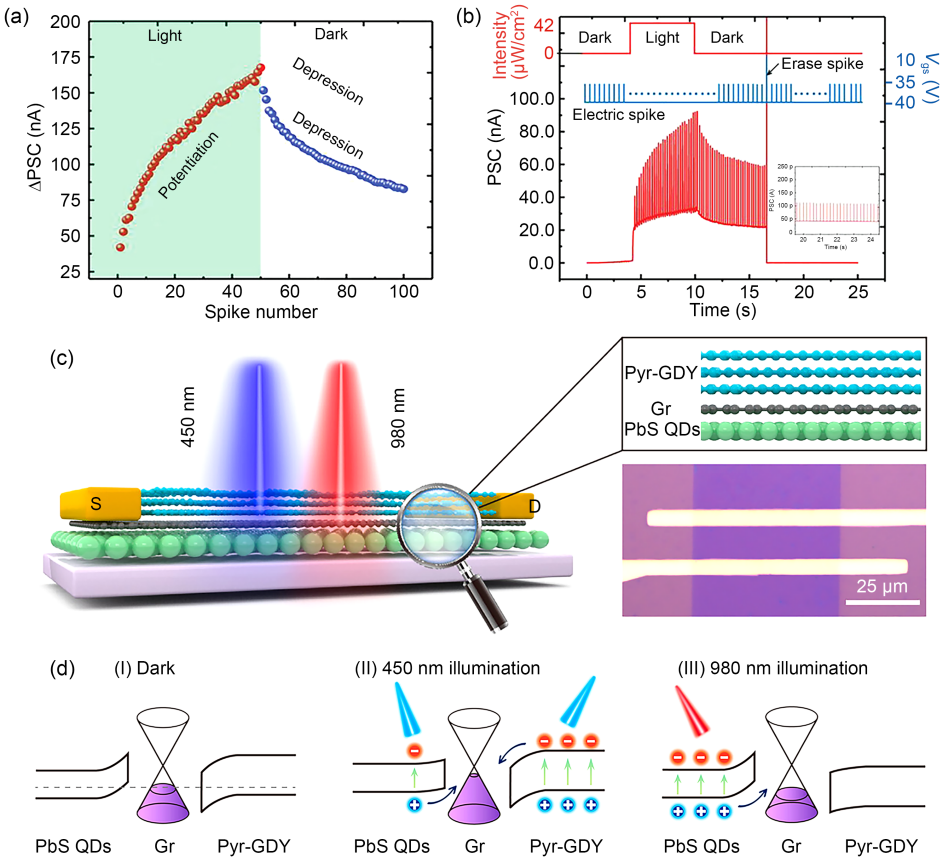

Fig. 10 (a) ΔPSC with and without optical signals; (b) erasing operation; (c) structure of the flexible device; (d) working mechanism of the flexible optical synapse. (a) and (b) are reprinted from Sun et al. (2021b), Copyright 2021, with permission from Wiley-VCH GmbH; (c) and (d) are reprinted from Hou et al. (2021), Copyright 2021, with permission from American Chemical Society

because of the recombination of photogenerated holes and intrinsic electrons in Gr. While 450 nm light can be absorbed by both PbS NCs and Pyr GDY, most is absorbed by Pyr GDY as it is on the top. Hence, in the Gr layer, photogenerated electrons transferred from Pyr GDY are much more than photogenerated holes transferred from PbS NCs, leading to higher electron level and greater conductivity. Lin et al. (2020) fabricated a flexible, all-carbon memristive synapse based on graphene oxide (GO) and NCNC nanocomposites, which realized A-RS. In contrast to the devices using PVP/NCNC nanocomposites fabricated by Zeng et al. (2021), A-RS with a gradual conductance change was achieved via reducing GO by applying ultraviolet light to the device in Lin et al. (2020). GO introduced into NCNC sheets worked as the reaction catalyst. Under ultraviolet irradiation, GO was excited. H_2O molecules (coming from the air) absorbed on it were decomposed into O_2 and H^+, leaving some electrons. Then the excited electrons in GO were transferred to NCNCs, leading to a local reduction. Their memristive synapse emulated synaptic functions such as EPSC, PPF, and STDP, and showed good flexibility and three-dimensional (3D) conformality. This can contribute to the development of wearable neuromorphic computing systems. The work of Lin et al. (2020) is a significant example of the integration of synaptic transistors based on NCs. A flexible device using nanostructured polycrystalline MoS_2 films synthesized on flexible substrates has also been reported (Lee E et al., 2020). All of these flexible devices exhibit strong working stability at bending states.

It is worth remarking that the combination of graphene and perovskite NCs may lead to amazing improvements in device performances. Pradhan et al. (2020) fabricated phototransistors based on graphene-perovskite NCs (G-PNCs), showing an excellent

responsivity of 1.4×10^8 A/W. The PPF index of synaptic devices using the heterostructure of graphene and perovskite NCs can be elevated to 196% (Han et al., 2022).

4.4 Heterojunction devices of NCs with other semiconductor materials

Typically, a large on-off ratio (the resistance ratio of the HRS to LRS) is regarded as an important standard for valuing memristors. A good example is the nonvolatile memristor with a high on-off ratio of 10^4 reported by Thomas et al. (2020). Molybdenum disulfide (MoS_2) NCs synthesized by the liquid-phase exfoliation method were used in this device.

For synaptic devices based on NCs, reliability is always a problem. The development of methods to improve device reliability and reduce variability is essential, but little such development has been reported. Yan XB et al. (2019) reported a memristor device (MD) with a self-assembled, networked PbS NC film. The use of NCs with a self-assemble ability makes possible a large on-off ratio, high uniformity, and remarkable responsiveness. Compared to no-NC memristor devices and isolated-quantum dot (IQD) devices, networked quantum dot (NQD) devices demonstrate the most concentrated switching threshold voltage, shortest response time, and best retention performance. The geometry of these devices is a simple Ag/Ga_2O_3/Pt multilayer structure, and the PbS NCs are deposited between the Ga_2O_3 and Pt film via drop casting. Sixty devices from three batches, selected randomly for each sample, are prepared, providing the electrical measurement results in Fig. 11. Figs. 11a, 11b, and 11c show the current-voltage (I–V) curves of pure Ga_2O_3 MDs, IQD MDs, and NQD MDs, respectively. Clearly, the NQD MDs exhibit the most reproducible performance among the three kinds of MDs. Further analysis shows that the distribution range of both the set and reset voltages of NQD MDs is about one order of magnitude lower than those of other MDs, which signifies that precise control of the programming voltage can be realized.

Figs. 11d–11f show the SET response time of three kinds of devices, which is approximately 43, 18, and 5.3 ns, respectively. The resistance distribution of HRS and LRS of these devices is plotted in Fig. 11g, which shows the most concentrated distribution of NQD MDs among the three. The energy consumption of the set and reset operations of these three kinds of devices and a comparison with data in the literature are shown in Figs. 11h and 11i. To further show the structure of these three kinds of devices, cross-sectional transmission electron microscope (TEM) images, high-resolution TEM images, and crystalline directions of selected areas are all shown in Fig. 12.

Yan XB et al. (2019) stated that the excellent performance of NQD MDs can be explained by the convergence of Ag clusters near the PbS NCs. The electric field lines converge around the NC sites, which enhances the localized electric field, causing the convergence of Ag ions and increasing the nucleation probability of Ag atoms. Under the strong localized electric field, the growth of Ag conductive filaments is promoted by the Ag nucleus (Buca et al., 2009; Liu Q et al., 2009). Rapid ion motion might come from the combined effects of the strong localized electric field and local current-induced high temperature, producing a fast response time (Choi et al., 2011).

Tunable resistive switching synaptic devices have also been reported. Zhang XN et al. (2019) reported a memory device based on all-inorganic $CsPbBr_3$ NCs, which exhibits a forming-free, bipolar resistive switching with a tunable on-off ratio from metastable 10^6 to stable 10. Additionally, this research suggests the tunable resistive switching of Au/poly(methyl methacrylate) (PMMA)/PMMA:$CsPbBr_3$ NCs/PMMA/ITO through light luminescence and the achievement of a controllable photo response.

5 Perspectives

The development of synaptic devices based on semiconductor NCs benefits both the research of artificial neural networks and the study of nanomaterials. Though we have made significant breakthroughs in this area, it is undoubtable that there is still much work to be done.

One of the most intractable problems is the unbalanced development between different types of devices. Utilization in artificial neural networks requires functional diversity and a wide conductance range, for which attempting the use of different kinds of materials is an appropriate approach. Although semiconductor NCs can exhibit many excellent properties alone,

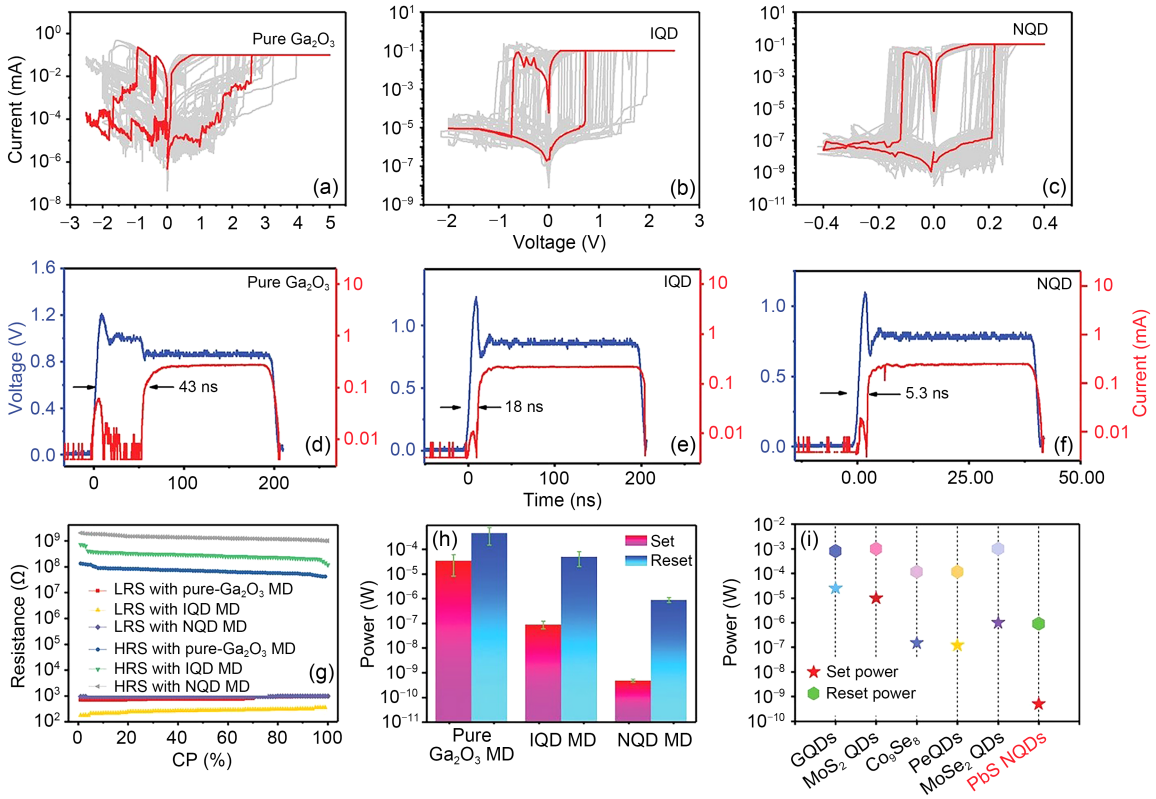

Fig. 11 Current-voltage (*I–V*) curves of pure Ga_2O_3 MDs (a), IQD MDs (b), and NQD MDs (c); SET response time for pure Ga_2O_3 MDs (d), IQD MDs (e), and NQD MDs (f); (g) resistance distribution for sweeping over 60 *I–V* cycles; (h) switching power of MDs; (i) comparison of device power with that in the literature. Reprinted from Yan XB et al. (2019), Copyright 2018, with permission from WILEY-VCH Verlag GmbH & Co. KGaA, Weinheim

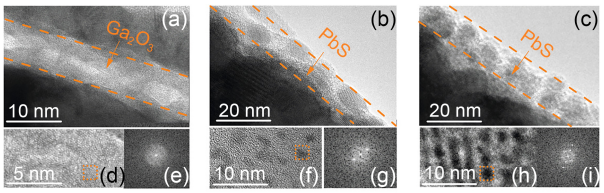

Fig. 12 Cross-sectional TEM images of pure Ga_2O_3 MDs (a), IQD MDs (b), and NQD MDs (c); high-resolution TEM images of pure Ga_2O_3 MDs (d), IQD MDs (f), and NQD MDs (h); (e), (g), and (i) are crystalline directions of the selected areas of (d), (f), and (h), respectively. Reprinted from Yan XB et al. (2019), Copyright 2018, with permission from WILEY-VCH Verlag GmbH & Co. KGaA, Weinheim

combining them with other materials such as ferroelectric materials and electrolyte crystals is the easiest way to increase device variety. Besides Si and perovskite NCs, other kinds of semiconductor NCs must be explored in depth.

The reliability of synaptic devices based on NCs is another important issue that could be solved by increasing the stability of NCs. Owing to their large specific surface area, semiconductor NCs are usually active and require particular environment conditions or even surface passivation. Some semiconductor NCs (such as perovskite NCs) suffer especially from poor chemical and thermal stability, which raises questions about their application. With the physical and chemical changes occurring during the use of synaptic devices, the limitation of instability may be magnified and may lead to a variation in device function, which not only impacts their large-scale application, but also makes it difficult to set a standard. Thus, handling this issue by methods such as surface modification, self-assembly technology, and encapsulation is essential. More feasible methods are also needed.

Another problem that requires attention before large-scale application in artificial neural networks is high-density integration. Though some examples we have mentioned show the potential of large-scale integration, there remains a need for strong architectural design, framework design, and a good match between

different types of devices based on NCs. How to match the inputs and outputs then becomes the first question to answer, suggesting the need to delve deeper into synaptic devices with optical output. The emergence of fully optical synaptic devices provides an interesting solution to this problem, but how to realize both light input and light output in devices remains a challenge.

6 Conclusions

In this review, we introduced semiconductor NCs and the synaptic devices based on them. The adjustable electronic, optical, and chemical properties make NCs an ideal material for memory devices and present broad application prospects in neuromorphic computing. A series of synaptic functionalities have been simulated, and many new regulation methods have been proposed.

However, synaptic devices based on NCs are confronted by many problems, such as device reliability, conductance range, and high-density integration. The nonuniformity and uncontrollable density of defects in NC solids strongly influence charge transport and trapping (Lv et al., 2020). Methods like self-assembly technology (Yan XB et al., 2019) and modulating ion migration by nanopores (Zhao XL et al., 2018) may solve this problem. In a crossbar structure, NCs can be easily integrated into the circuit, but device variation can be an obstacle.

For their ultimate use in artificial neural networks, the performance of synaptic devices based on semiconductor NCs must be further improved. To this end, further investigation of the physical mechanisms of synaptic devices based on semiconductor NCs is necessary. In conclusion, the development of fully optical synaptic devices using semiconductor NCs holds strong potential (Hu LX et al., 2021). However, challenges such as wavelength conversion, structure design, and signal attenuation on the path remain to be overcome.

Contributors

Mingxuan BU drafted the paper. Yue WANG and Xiaodong PI helped organize the paper. All authors contributed to the revision of the work. Mingxuan BU finalized the paper.

Compliance with ethics guidelines

Mingxuan BU, Yue WANG, Lei YIN, Zhouyu TONG, Yiqiang ZHANG, Deren YANG, and Xiaodong PI declare that they have no conflict of interest.

References

Arduca E, Perego M, 2017. Doping of silicon nanocrystals. *Mater Sci Semicond Process*, 62:156-170. https://doi.org/10.1016/j.mssp.2016.10.054

Attwell D, Laughlin SB, 2001. An energy budget for signaling in the grey matter of the brain. *J Cereb Blood Flow Metab*, 21(10):1133-1145. https://doi.org/10.1097/00004647-200110000-00001

Block N, 1981. Psychologism and behaviorism. *Philos Rev*, 90(1):5-43. https://doi.org/10.2307/2184371

Boles MA, Ling DS, Hyeon T, et al., 2016. The surface science of nanocrystals. *Nat Mater*, 15:141-153. https://doi.org/10.1038/nmat4526

Buca D, Minamisawa RA, Trinkaus H, et al., 2009. Relaxation of strained pseudomorphic Si_xGe_{1-x} layers on He-implanted Si/δ-Si: C/Si(100) substrates. *Appl Phys Lett*, 95(14):144103. https://doi.org/10.1063/1.3240409

Bussian DA, Crooker SA, Yin M, et al., 2009. Tunable magnetic exchange interactions in manganese-doped inverted core-shell ZnSe-CdSe nanocrystals. *Nat Mater*, 8(1):35-40. https://doi.org/10.1038/nmat2342

Chaudhuri RG, Paria S, 2012. Core/shell nanoparticles: classes, properties, synthesis mechanisms, characterization, and applications. *Chem Rev*, 112(4):2373-2433. https://doi.org/10.1021/cr100449n

Chen JY, Yang DL, Jhuang FC, et al., 2021. Ultrafast responsive and low-energy-consumption poly(3-hexylthiophene)/perovskite quantum dots composite film-based photonic synapse. *Adv Funct Mater*, 31(47):2105911. https://doi.org/10.1002/adfm.202105911

Chiu MY, Chen CC, Sheu JT, et al., 2009. An optical programming/electrical erasing memory device: organic thin film transistors incorporating core/shell CdSe@ZnSe quantum dots and poly(3-hexylthiophene). *Org Electron*, 10(5):769-774. https://doi.org/10.1016/j.orgel.2009.03.011

Choi BJ, Chen ABK, Yang X, et al., 2011. Purely electronic switching with high uniformity, resistance tunability, and good retention in Pt-dispersed SiO_2 thin films for ReRAM. *Adv Mater*, 23(33):3847-3852. https://doi.org/10.1002/adma.201102132

Coe S, Woo WK, Bawendi M, et al., 2002. Electroluminescence from single monolayers of nanocrystals in molecular organic devices. *Nature*, 420 (6917):800-803. https://doi.org/10.1038/nature01217

Collier CP, Saykally RJ, Shiang JJ, et al., 1997. Reversible tuning of silver quantum dot monolayers through the metal-insulator transition. *Science*, 277(5334):1978-1981. https://doi.org/10.1126/science.277.5334.1978

Dai SL, Zhao YW, Wang Y, et al., 2019. Recent advances in transistor-based artificial synapses. *Adv Funct Mater*, 29(42):1903700. https://doi.org/10.1002/adfm.201903700

D'amour JA, Froemke RC, 2015. Inhibitory and excitatory

spike-timing-dependent plasticity in the auditory cortex. *Neuron*, 86(2):514-528. https://doi.org/10.1016/j.neuron.2015.03.014

Dasog M, De Los Reyes GB, Titova LV, et al., 2014. Size vs surface: tuning the photoluminescence of freestanding silicon nanocrystals across the visible spectrum via surface groups. *ACS Nano*, 8(9):9636-9648. https://doi.org/10.1021/nn504109a

Debanne D, Guérineau NC, Gähwiler BH, et al., 1996. Paired-pulse facilitation and depression at unitary synapses in rat hippocampus: quantal fluctuation affects subsequent release. *J Physiol*, 491(1):163-176. https://doi.org/10.1113/jphysiol.1996.sp021204

Deegan RD, Bakajin O, Dupont TF, et al., 1997. Capillary flow as the cause of ring stains from dried liquid drops. *Nature*, 389(6653):827-829. https://doi.org/10.1038/39827

Dohnalová K, Gregorkiewicz T, Kůsová K, 2014. Silicon quantum dots: surface matters. *J Phys Condens Matter*, 26(17): 173201. https://doi.org/10.1088/0953-8984/26/17/173201

Ekimov AI, Efros AL, Onushchenko AA, 1985. Quantum size effect in semiconductor microcrystals. *Sol State Commun*, 56(11):921-924. https://doi.org/10.1016/S0038-1098(85)80025-9

Erogbogbo F, Liu TH, Ramadurai N, et al., 2011. Creating ligand-free silicon germanium alloy nanocrystal inks. *ACS Nano*, 5(10):7950-7959. https://doi.org/10.1021/nn2023304

Esser SK, Merolla PA, Arthur JV, et al., 2016. Convolutional networks for fast, energy-efficient neuromorphic computing. *Proc Natl Acad Sci USA*, 113(41):11441-11446. https://doi.org/10.1073/pnas.1604850113

Gkoupidenis P, Koutsouras DA, Malliaras GG, 2017. Neuromorphic device architectures with global connectivity through electrolyte gating. *Nat Commun*, 8(1):15448. https://doi.org/10.1038/ncomms15448

Guo LJ, Leobandung E, Chou SY, 1997. A silicon single-electron transistor memory operating at room temperature. *Science*, 275(5300):649-651. https://doi.org/10.1126/science.275.5300.649

Gur I, Fromer NA, Geier ML, et al., 2005. Air-stable all-inorganic nanocrystal solar cells processed from solution. *Science*, 310(5747):462-465. https://doi.org/10.1126/science.1117908

Han C, Han XW, Han JY, et al., 2022. Light-stimulated synaptic transistor with high PPF feature for artificial visual perception system application. *Adv Funct Mater*, 32(22): 2113053. https://doi.org/10.1002/adfm.202113053

Hao DD, Zhang JY, Dai SL, et al., 2020. Perovskite/organic semiconductor-based photonic synaptic transistor for artificial visual system. *ACS Appl Mater Interf*, 12(35): 39487-39495. https://doi.org/10.1021/acsami.0c10851

He LH, Li EL, He WX, et al., 2021. Complementary of ferroelectric and floating gate structure for high performance organic nonvolatile memory. *Adv Electron Mater*, 7(11): 2100599. https://doi.org/10.1002/aelm.202100599

He WX, Fang Y, Yang HH, et al., 2019. A multi-input light-stimulated synaptic transistor for complex neuromorphic computing. *J Mater Chem C*, 7(40):12523-12531. https://doi.org/10.1039/c9tc03898a

Heitmann J, Müller F, Zacharias M, et al., 2005. Silicon nanocrystals: size matters. *Adv Mater*, 17(7):795-803. https://doi.org/10.1002/adma.200401126

Holman ZC, Kortshagen UR, 2011. Nanocrystal inks without ligands: stable colloids of bare germanium nanocrystals. *Nano Lett*, 11(5):2133-2136. https://doi.org/10.1021/nl200774y

Hou YX, Li Y, Zhang ZC, et al., 2021. Large-scale and flexible optical synapses for neuromorphic computing and integrated visible information sensing memory processing. *ACS Nano*, 15(1):1497-1508. https://doi.org/10.1021/acsnano.0c08921

Hu H, Larson RG, 2005. Analysis of the effects of marangoni stresses on the microflow in an evaporating sessile droplet. *Langmuir*, 21(9):3972-3980. https://doi.org/10.1021/la0475270

Hu H, Wen GH, Wen JM, et al., 2021. Ambipolar charge storage in type-I core/shell semiconductor quantum dots toward optoelectronic transistor-based memories. *Adv Sci*, 8(16):2100513. https://doi.org/10.1002/advs.202100513

Hu LX, Yang J, Wang JR, et al., 2021. All-optically controlled memristor for optoelectronic neuromorphic computing. *Adv Funct Mater*, 31(4):2005582. https://doi.org/10.1002/adfm.202005582

Huang W, Hang PJ, Wang Y, et al., 2020. Zero-power optoelectronic synaptic devices. *Nano Energy*, 73:104790. https://doi.org/10.1016/j.nanoen.2020.104790

Hussain T, Abbas H, Youn C, et al., 2022. Cellulose nanocrystal based bio-memristor as a green artificial synaptic device for neuromorphic computing applications. *Adv Mater Technol*, 7(2):2100744. https://doi.org/10.1002/admt.202100744

Indiveri G, Chicca E, Douglas R, 2006. A VLSI array of low-power spiking neurons and bistable synapses with spike-timing dependent plasticity. *IEEE Trans Neur Netw*, 17(1): 211-221. https://doi.org/10.1109/TNN.2005.860850

Jiang CB, Zhong ZM, Liu BQ, et al., 2016. Coffee-ring-free quantum dot thin film using inkjet printing from a mixed-solvent system on modified ZnO transport layer for light-emitting devices. *ACS Appl Mater Interf*, 8(39):26162-26168. https://doi.org/10.1021/acsami.6b08679

Kagan CR, Lifshitz E, Sargent EH, et al., 2016. Building devices from colloidal quantum dots. *Science*, 353(6302): aac5523. https://doi.org/10.1126/science.aac5523

Kawauchi T, Kano S, Fujii M, 2019. Electrically stimulated synaptic resistive switch in solution-processed silicon nanocrystal thin film: formation mechanism of oxygen vacancy filament for synaptic function. *ACS Appl Electron Mater*, 1(12):2664-2670. https://doi.org/10.1021/acsaelm.9b00625

Kim K, Chen CL, Truong Q, et al., 2013. A carbon nanotube synapse with dynamic logic and learning. *Adv Mater*, 25(12): 1693-1698. https://doi.org/10.1002/adma.201203116

Lee E, Kim J, Bhoyate S, et al., 2020. Realizing scalable two-dimensional MoS_2 synaptic devices for neuromorphic computing. *Chem Mater*, 32(24):10447-10455. https://doi.org/10.1021/acs.chemmater.0c03112

Lee WCA, Bonin V, Reed M, et al., 2016. Anatomy and function of an excitatory network in the visual cortex. *Nature*, 532(7599):370-374. https://doi.org/10.1038/nature17192

Li EL, Lin WK, Yan YJ, et al., 2019. Synaptic transistor capable of accelerated learning induced by temperature-facilitated modulation of synaptic plasticity. *ACS Appl Mater Interf*, 11(49):46008-46016. https://doi.org/10.1021/acsami.9b17227

Li FS, Son DI, Seo SM, et al., 2007. Organic bistable devices based on core/shell CdSe/ZnS nanoparticles embedded in a conducting poly(*N*-vinylcarbazole) polymer layer. *Appl Phys Lett*, 91(12):122111. https://doi.org/10.1063/1.2783189

Li Q, Luo TY, Zhou M, et al., 2016. Silicon nanoparticles with surface nitrogen: 90% quantum yield with narrow luminescence bandwidth and the ligand structure based energy law. *ACS Nano*, 10(9):8385-8393. https://doi.org/10.1021/acsnano.6b03113

Li XM, Rui MC, Song JZ, et al., 2015. Carbon and graphene quantum dots for optoelectronic and energy devices: a review. *Adv Funct Mater*, 25(31):4929-4947. https://doi.org/10.1002/adfm.201501250

Li YY, Wang Y, Yin L, et al., 2021. Silicon-based inorganic-organic hybrid optoelectronic synaptic devices simulating cross-modal learning. *Sci China Inform Sci*, 64(6): 162401. https://doi.org/10.1007/s11432-020-3035-8

Lin Y, Wang ZQ, Zhang X, et al., 2020. Photoreduced nanocomposites of graphene oxide/N-doped carbon dots toward all-carbon memristive synapses. *NPG Asia Mater*, 12(1): 64. https://doi.org/10.1038/s41427-020-00245-0

Liu CS, Yan X, Song XF, et al., 2018. A semi-floating gate memory based on van der Waals heterostructures for quasi-non-volatile applications. *Nat Nanotechnol*, 13(5): 404-410. https://doi.org/10.1038/s41565-018-0102-6

Liu Q, Dou CM, Wang Y, et al., 2009. Formation of multiple conductive filaments in the Cu/ZrO_2: Cu/Pt device. *Appl Phys Lett*, 95(2):023501. https://doi.org/10.1063/1.3176977

Liu XK, Zhang YH, Yu T, et al., 2016. Optimum quantum yield of the light emission from 2 to 10 nm hydrosilylated silicon quantum dots. *Part Part Syst Charact*, 33(1):44-52. https://doi.org/10.1002/ppsc.201500148

Liu Y, Gibbs M, Puthussery J, et al., 2010. Dependence of carrier mobility on nanocrystal size and ligand length in PbSe nanocrystal solids. *Nano Lett*, 10(5):1960-1969. https://doi.org/10.1021/nl101284k

Lv ZY, Wang Y, Chen JR, et al., 2020. Semiconductor quantum dots for memories and neuromorphic computing systems. *Chem Rev*, 120(9):3941-4006. https://doi.org/10.1021/acs.chemrev.9b00730

Ma HL, Wang W, Xu HY, et al., 2018. Interface state-induced negative differential resistance observed in hybrid perovskite resistive switching memory. *ACS Appl Mater Interf*, 10(25):21755-21763. https://doi.org/10.1021/acsami.8b07850

Ma YS, Pi XD, Yang DR, 2012. Fluorine-passivated silicon nanocrystals: surface chemistry versus quantum confinement. *J Phys Chem C*, 116(9):5401-5406. https://doi.org/10.1021/jp211177d

Machens CK, 2012. Building the human brain. *Science*, 338(6111):1156-1157. https://doi.org/10.1126/science.1231865

Manipatruni S, Nikonov DE, Young IA, 2018. Beyond CMOS computing with spin and polarization. *Nat Phys*, 14(4): 338-343. https://doi.org/10.1038/s41567-018-0101-4

Marri I, Degoli E, Ossicini S, 2017. Doped and codoped silicon nanocrystals: the role of surfaces and interfaces. *Prog Surf Sci*, 92(4):375-408. https://doi.org/10.1016/j.progsurf.2017.07.003

Mastronardi ML, Maier-Flaig F, Faulkner D, et al., 2012. Size-dependent absolute quantum yields for size-separated colloidally-stable silicon nanocrystals. *Nano Lett*, 12(1): 337-342. https://doi.org/10.1021/nl2036194

Merolla PA, Arthur JV, Alvarez-Icaza R, et al., 2014. A million spiking-neuron integrated circuit with a scalable communication network and interface. *Science*, 345(6197):668-673. https://doi.org/10.1126/science.1254642

Ni ZY, Pi XD, Zhou S, et al., 2016. Size-dependent structures and optical absorption of boron-hyperdoped silicon nanocrystals. *Adv Opt Mater*, 4(5):700-707. https://doi.org/10.1002/adom.201500706

Ni ZY, Ma LL, Du SC, et al., 2017. Plasmonic silicon quantum dots enabled high-sensitivity ultrabroadband photodetection of graphene-based hybrid phototransistors. *ACS Nano*, 11(10):9854-9862. https://doi.org/10.1021/acsnano.7b03569

Ni ZY, Wang Y, Liu LX, et al., 2018. Hybrid structure of silicon nanocrystals and 2D WSe_2 for broadband optoelectronic synaptic devices. IEEE Int Electron Devices Meeting, p.38.5.1-38.5.4. https://doi.org/10.1109/IEDM.2018.8614657

Ni ZY, Zhou S, Zhao SY, et al., 2019. Silicon nanocrystals: unfading silicon materials for optoelectronics. *Mater Sci Eng R Rep*, 138:85-117. https://doi.org/10.1016/j.mser.2019.06.001

Norris DJ, Efros AL, Erwin SC, 2008. Doped nanocrystals. *Science*, 319(5871):1776-1779. https://doi.org/10.1126/science.1143802

Periyal SS, Jagadeeswararao M, Ng SE, et al., 2020. Halide perovskite quantum dots photosensitized-amorphous oxide transistors for multimodal synapses. *Adv Mater Technol*, 5(11):2000514. https://doi.org/10.1002/admt.202000514

Pradhan B, Das S, Li JX, et al., 2020. Ultrasensitive and ultrathin phototransistors and photonic synapses using perovskite quantum dots grown from graphene lattice. *Sci Adv*, 6(7): eaay5225. https://doi.org/10.1126/sciadv.aay5225

Prezioso M, Merrikh-Bayat F, Hoskins BD, et al., 2015. Training and operation of an integrated neuromorphic network based on metal-oxide memristors. *Nature*, 521(7550):61-64. https://doi.org/10.1038/nature14441

Schaller RD, Klimov VI, 2004. High efficiency carrier multiplication in PbSe nanocrystals: implications for solar energy conversion. *Phys Rev Lett*, 92(18):186601. https://doi.org/10.1103/PhysRevLett.92.186601

Schaller RD, Agranovich VM, Klimov VI, 2005. High-efficiency carrier multiplication through direct photogeneration of multi-excitons via virtual single-exciton states. *Nat Phys*, 1(3):189-194. https://doi.org/10.1038/nphys151

Searle JR, 1980. Minds, brains, and programs. *Behav Brain Sci*, 3(3):417-424. https://doi.org/10.1017/S0140525X00005756

Semonin OE, Johnson JC, Luther JM, et al., 2010. Absolute photoluminescence quantum yields of IR-26 dye, PbS, and PbSe quantum dots. *J Phys Chem Lett*, 1(16):2445-2450. https://doi.org/10.1021/jz100830r

Service RF, 2004. Printable electronics that stick around. *Science*, 304(5671):675. https://doi.org/10.1126/science.304.5671.675

Singh M, Goyal M, Devlal K, 2018. Size and shape effects on the band gap of semiconductor compound nanomaterials. *J Taibah Univ Sci*, 12(4):470-475. https://doi.org/10.1080/16583655.2018.1473946

Smith AM, Nie SM, 2010. Semiconductor nanocrystals: structure, properties, and band gap engineering. *Acc Chem Res*, 43(2):190-200. https://doi.org/10.1021/ar9001069

So WY, Li Q, Legaspi CM, et al., 2018. Mechanism of ligand-controlled emission in silicon nanoparticles. *ACS Nano*, 12(7):7232-7238. https://doi.org/10.1021/acsnano.8b03273

Sonawane KG, Rajesh C, Temgire M, et al., 2011. A case study: Te in ZnSe and Mn-doped ZnSe quantum dots. *Nanotechnology*, 22(30):305702. https://doi.org/10.1088/0957-4484/22/30/305702

Sun YL, Ding YT, Xie D, 2021a. Mixed-dimensional van der Waals heterostructures enabled optoelectronic synaptic devices for neuromorphic applications. *Adv Funct Mater*, 31(47):2105625. https://doi.org/10.1002/adfm.202105625

Sun YL, Ding YT, Xie D, et al., 2021b. Optogenetics-inspired neuromorphic optoelectronic synaptic transistors with optically modulated plasticity. *Adv Opt Mater*, 9(12):2002232. https://doi.org/10.1002/adom.202002232

Talapin DV, Murray CB, 2005. PbSe nanocrystal solids for n- and p-channel thin film field-effect transistors. *Science*, 310(5745):86-89. https://doi.org/10.1126/science.1116703

Talgorn E, Gao YN, Aerts M, et al., 2011. Unity quantum yield of photogenerated charges and band-like transport in quantum-dot solids. *Nat Nanotechnol*, 6(11):733-739. https://doi.org/10.1038/nnano.2011.159

Tan H, Ni ZY, Peng WB, et al., 2018. Broadband optoelectronic synaptic devices based on silicon nanocrystals for neuromorphic computing. *Nano Energy*, 52:422-430. https://doi.org/10.1016/j.nanoen.2018.08.018

Tang JS, Yuan F, Shen XK, et al., 2019. Bridging biological and artificial neural networks with emerging neuromorphic devices: fundamentals, progress, and challenges. *Adv Mater*, 31(49):1902761. https://doi.org/10.1002/adma.201902761

Thomas A, Resmi AN, Ganguly A, et al., 2020. Programmable electronic synapse and nonvolatile resistive switches using MoS_2 quantum dots. *Sci Rep*, 10(1):12450. https://doi.org/10.1038/s41598-020-68822-5

Turing AM, 1950. Computing machinery and intelligence. *Mind*, 59(236):433-460.

Upadhyay NK, Joshi S, Yang JJ, 2016. Synaptic electronics and neuromorphic computing. *Sci China Inform Sci*, 59(6):061404. https://doi.org/10.1007/s11432-016-5565-1

van de Burgt Y, Melianas A, Keene ST, et al., 2018. Organic electronics for neuromorphic computing. *Nat Electron*, 1(7):386-397. https://doi.org/10.1038/s41928-018-0103-3

Wang K, Dai SL, Zhao YW, et al., 2019. Light-stimulated synaptic transistors fabricated by a facile solution process based on inorganic perovskite quantum dots and organic semiconductors. *Small*, 15(11):1900010. https://doi.org/10.1002/smll.201900010

Wang Q, Shao YC, Xie HP, et al., 2014. Qualifying composition dependent *p* and *n* self-doping in $CH_3NH_3PbI_3$. *Appl Phys Lett*, 105(16):163508. https://doi.org/10.1063/1.4899051

Wang R, Pi XD, Yang DR, 2012. First-principles study on the surface chemistry of 1.4 nm silicon nanocrystals: case of hydrosilylation. *J Phys Chem C*, 116(36):19434-19443. https://doi.org/10.1021/jp307785v

Wang TY, Meng JL, Rao MY, et al., 2020. Three-dimensional nanoscale flexible memristor networks with ultralow power for information transmission and processing application. *Nano Lett*, 20(6):4111-4120. https://doi.org/10.1021/acs.nanolett.9b05271

Wang Y, Lv ZY, Chen JR, et al., 2018. Photonic synapses based on inorganic perovskite quantum dots for neuromorphic computing. *Adv Mater*, 30(38):1802883. https://doi.org/10.1002/adma.201802883

Wang Y, Yin L, Huang W, et al., 2021. Optoelectronic synaptic devices for neuromorphic computing. *Adv Intell Syst*, 3(1):2000099. https://doi.org/10.1002/aisy.202000099

Wang Y, Zhu YY, Li YY, et al., 2022. Dual-modal optoelectronic synaptic devices with versatile synaptic plasticity. *Adv Funct Mater*, 32(1):2107973. https://doi.org/10.1002/adfm.202107973

Wang ZQ, Zeng T, Ren YY, et al., 2020. Toward a generalized Bienenstock-Cooper-Munro rule for spatiotemporal learning via triplet-STDP in memristive devices. *Nat Commun*, 11(1):1510. https://doi.org/10.1038/s41467-020-15158-3

Yan CY, Wen JM, Lin P, et al., 2019. A tunneling dielectric layer free floating gate nonvolatile memory employing type-I core–shell quantum dots as discrete charge-trapping/tunneling centers. *Small*, 15(1):1804156. https://doi.org/10.1002/smll.201804156

Yan XB, Pei YF, Chen HW, et al., 2019. Self-assembled networked PbS distribution quantum dots for resistive switching and artificial synapse performance boost of memristors. *Adv Mater*, 31(7):1805284. https://doi.org/10.1002/adma.201805284

Yang FQ, 2021. Size effect on the bandgap change of quantum dots: thermomechanical deformation. *Phys Lett A*, 401:127346. https://doi.org/10.1016/j.physleta.2021.127346

Yang J, Choi MK, Kim DH, et al., 2016. Designed assembly and integration of colloidal nanocrystals for device applications. *Adv Mater*, 28(6):1176-1207. https://doi.org/10.1002/adma.201502851

Yin L, Han C, Zhang QT, et al., 2019. Synaptic silicon-nanocrystal phototransistors for neuromorphic computing. *Nano Energy*, 63:103859. https://doi.org/10.1016/j.nanoen.2019.103859

Yin L, Pi XD, Yang DR, 2020. Silicon-based optoelectronic synaptic devices. *Chin Phys B*, 29(7):070703. https://doi.org/10.1088/1674-1056/ab973f

Yu JS, Kim I, Kim JS, et al., 2012. Silver front electrode grids for ITO-free all printed polymer solar cells with embedded

and raised topographies, prepared by thermal imprint, flexographic and inkjet roll-to-roll processes. *Nanoscale*, 4(19):6032-6040. https://doi.org/10.1039/c2nr31508d

Zeng T, Yang Z, Liang JB, et al., 2021. Flexible and transparent memristive synapse based on polyvinylpyrrolidone/N-doped carbon quantum dot nanocomposites for neuromorphic computing. *Nanoscale Adv*, 3(9):2623-2631. https://doi.org/10.1039/D1NA00152C

Zhang H, Zhang YT, Yu Y, et al., 2017. Ambipolar quantum-dot-based low-voltage nonvolatile memory with double floating gates. *ACS Photon*, 4(9):2220-2227. https://doi.org/10.1021/acsphotonics.7b00416

Zhang XN, Yang HY, Jiang ZG, et al., 2019. Photoresponse of nonvolatile resistive memory device based on all-inorganic perovskite $CsPbBr_3$ nanocrystals. *J Phys D Appl Phys*, 52(12):125103. https://doi.org/10.1088/1361-6463/aafe8e

Zhao SY, Ni ZY, Tan H, et al., 2018a. Electroluminescent synaptic devices with logic functions. *Nano Energy*, 54:383-389. https://doi.org/10.1016/j.nanoen.2018.10.018

Zhao SY, Liu XK, Pi XD, et al., 2018b. Light-emitting diodes based on colloidal silicon quantum dots. *J Semicond*, 39(6):061008. https://doi.org/10.1088/1674-4926/39/6/061008

Zhao SY, Wang Y, Huang W, et al., 2019. Developing near-infrared quantum-dot light-emitting diodes to mimic synaptic plasticity. *Sci China Mater*, 62(10):1470-1478. https://doi.org/10.1007/s40843-019-9437-9

Zhao XL, Ma J, Xiao XH, et al., 2018. Breaking the current-retention dilemma in cation-based resistive switching devices utilizing graphene with controlled defects. *Adv Mater*, 30(14):1705193. https://doi.org/10.1002/adma.201705193

Zhao XN, Wang ZQ, Li WT, et al., 2020. Photoassisted electroforming method for reliable low-power organic–inorganic perovskite memristors. *Adv Funct Mater*, 30(17):1910151. https://doi.org/10.1002/adfm.201910151

Zhou S, Ni ZY, Ding Y, et al., 2016. Ligand-free, colloidal, and plasmonic silicon nanocrystals heavily doped with boron. *ACS Photon*, 3(3):415-422. https://doi.org/10.1021/acsphotonics.5b00568

Zhu LQ, Xiao H, Liu YH, et al., 2015. Multi-gate synergic modulation in laterally coupled synaptic transistors. *Appl Phys Lett*, 107(14):143502. https://doi.org/10.1063/1.4932568

Zhu YB, Wu CX, Xu ZW, et al., 2021. Light-emitting memristors for optoelectronic artificial efferent nerve. *Nano Lett*, 21(14):6087-6094. https://doi.org/10.1021/acs.nanolett.1c01482

Zhu YY, Huang W, He YF, et al., 2020. Perovskite-enhanced silicon-nanocrystal optoelectronic synaptic devices for the simulation of biased and correlated random-walk learning. *Research*, 2020:7538450. https://doi.org/10.34133/2020/7538450

Zidan MA, Strachan JP, Lu WD, 2018. The future of electronics based on memristive systems. *Nat Electron*, 1(1):22-29. https://doi.org/10.1038/s41928-017-0006-8

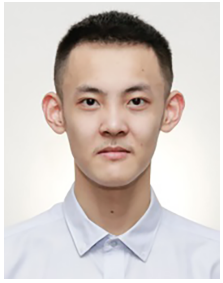

Mingxuan BU, first author of this invited paper, received his BS degree in the School of Materials Science and Engineering at Zhejiang University in 2021. He is now pursuing his MS degree at the State Key Laboratory of Silicon Materials at Zhejiang University. He is currently investigating optoelectronic synaptic devices based on semiconductor nanocrystals.

Xiaodong PI, corresponding author of this invited paper, received his PhD degree at the University of Bath in 2004. He then carried out research at McMaster University and the University of Minnesota at Twin Cities. He joined Zhejiang University as an associate professor in 2008. He is now a professor at the State Key Laboratory of Silicon Materials, School of Materials Science and Engineering and Hangzhou Innovation Center at Zhejiang University. Prof. PI is a corresponding expert of *Front Inform Technol Electron Eng*. His research interest concerns mainly group IV semiconductor materials and devices.